DTIC FILE COPY

(1)

AD-A202 707

DTIC
S ELECTE D
JAN 1 8 1989
H

DEPARTMENT OF THE AIR FORCE

AIR UNIVERSITY

AIR FORCE INSTITUTE OF TECHNOLOGY

Wright-Patterson Air Force Base, Ohio

DISTRIBUTION STATEMENT A

Approved for public release;
Distribution Unlimited

89 1 17 899

1

AFIT/GAE/AA/88D-27

AN EXPERIMENTAL INVESTIGATION OF FLOW MIXING ON THRUST EJECTOR EFFICIENCY

THESIS

Donald J. Morfitt, Jr.
Captain, USAF

AFIT/GAE/AA/88D-27

Approved for public release; distribution unlimited

AFIT/GAE/AA/88D-27

AN EXPERIMENTAL INVESTIGATION OF FLOW MIXING ON THRUST EJECTOR EFFICIENCY

THESIS

Presented to the Faculty of the School of Engineering

of the Air Force Institute of Technology

Air University

In Partial Fulfillment of the

Requirements for the Degree of

Master of Science in Aerospace Engineering

Donald J. Morfitt, Jr., B.S.

Captain, USAF

December 1988

Preface

The purpose of this investigation was to determine the effect flow mixing would have on the thrust augmentation of a 4.4 inch diameter circular ejector. This was accomplished by changing the angle of the primary nozzle tips with respect to the inlet surface of the ejector. The angle change was studied in an effort to promote flow mixing or swirling. Also studied was the effect primary flow pulsation has on the thrust augmentation ratio. This study was a continuation of studies previously done by Captains Reznick, Unnever, Lewis, and Uhuad.

I would like to thank several people that provided the valuable and needed assistance for me to complete this investigation.

- Dr. M. E. Franke, my thesis advisor, for his advice and suggestions in studying thrust augmentation.
- Dr. W. Elrod and Capt J. Planeaux, members of my thesis committee.
- Mr. N. Yardich, Mr. L. Cannon, and Mr. G. Hild for their assistance in the aerospace department laboratory.
- Mr. R. Biddle for his help in manufacturing the primary nozzles needed in this investigation.
- A special thanks goes to Mr. J. Anderson for his ideas on how to pulse the primary nozzle flow and allowing me to accomplish the experiments required to complete my masters thesis.

Donald J. Morfitt, Jr.

Table of Contents

List of Figures

List of Tables

List of Symbols

A	Area (in^2)
A_o	Primary Nozzle Area (in^2)
A_1	Inlet Area (in^2)
A_2	Mixing Chamber Cross Sectional Area (in^2)
A_3	Diffuser Exit Cross Sectional Area (in^2)
c	Discharge Coefficient (ft/s^2)
C_p	Pressure Coefficient
d	Diameter of Mass Flow Orifice (in)
F_a	Area Thermal Expansion Factor
F_i	Isentropic Thrust (lbf)
F_m	Measured Thrust (lbf)
h	Primary Nozzle Height (in)
Hz	hertz (cycles/sec)
M	Mass Augmentation Ratio
M	Mach Number
$\dot{m}_1$	Primary Air Mass Flow Rate (lbm/sec)
$\dot{m}_2$	Secondary Air Mass Flow Rate (lbm/sec)
$\dot{m}_3$	Ejector Exit Plane Mass Flow Rate (lbm/sec)
P_a	Atmospheric Pressure
P_s	Static Pressure
P_1	Pressure Before Mass Flow Orifice (lbf/in^2)
P_2	Pressure After Mass Flow Orifice (lbf/in^2)
q	Quality of Ejector
q_i	Ideal Quality of Ejector
$\Delta q/q_i$	Measure of Duct-Diffuser Losses

V_e	Velocity of Moving Ejector (ft/sec)
V_i	Isentropic Velocity (ft/sec)
V_m	Measured Velocity (ft/sec)
V_o	Primary Nozzle Velocity (ft/sec)
V_1	Inlet Flow Velocity (ft/sec)
V_2	Mixing Chamber Exit Velocity (ft/sec)
V_3	Diffuser Exit Velocity (ft/sec)
y	Expansion Factor for Air
α	Primary Nozzle Injection Angle (deg)
α	Primary to Inlet Area Ratio (A_o/A_1)
β	Diffuser to Mixing Chamber Area Ratio (A_3/A_2)
β_3	Flow Skewness Measure
β^*	Ratio of Diameters
ε_1	Inlet Loss Coefficient
ε_2	Wall Friction Coefficient
γ	Specific Heat Ratio
η_n	Primary Nozzle Efficiency
θ	Primary Nozzle Exit Location (deg)
ϕ	Thrust Augmentation Ratio
ρ	Density (slug/ft^3)

Abstract

The purpose of this study was to determine the effect flow mixing has on the thrust augmentation of an ejector. The experimental studies were divided into four phases. The four phases were baseline verification, a nozzle tip inclination study, a primary flow pulsing study, and a study of the quality of the ejector.

The baseline verification study showed thrust augmentation is dependent upon the injection angle and height of the primary nozzles. The nozzle tip inclination study investigated the effects of having the tips inclined from the inlet surface of the ejector. The nozzle tips were inclined in four different configurations. The different configurations established a baseline or attempted to promote flow mixing and swirling. The best thrust augmentation was achieved when the nozzle tips were parallel to the inlet surface of the ejector. For the third phase, the primary air was pulsed at frequencies up to 15 hertz. The flow pulsing of the primary air enhanced flow mixing and increased thrust augmentation. The ejector efficiency study determined an approximate quality or efficiency value of the thrust ejector. When compared to an efficiency value achieved by Quinn, the ejector used in this study had four times the losses of his ejector. However, his ejector was four times longer.

AN EXPERIMENTAL INVESTIGATION OF FLOW MIXING ON THRUST EJECTOR EFFICIENCY

I. Introduction

Background

Theodore von Karman stated, "... considerations clearly show the necessity for more systematic experimental and theoretical investigations." of a thrust augmenting ejector (1:461-468). He had just explained the differences in calculating the thrust augmentation ratio of the traditional center blowing ejector (Fig. 1) to the then "new" method of blowing primary air next to the inlet wall (Fig. 2). Since then, the references in the bibliography show research has been conducted on the effects the primary to inlet area ratio, mixing chamber length, diffuser to mixing chamber cross sectional area ratio, and flow mixing have on the thrust augmentation ratio.

Much of this research was conducted for the purpose of integrating a workable concept into a vertical or short takeoff aircraft (V/STOL). To date, the only U.S. military aircraft designed for V/STOL and placed in operation is the AV-8 A/B Harrier (2:117, 281). The AV-8 obtains its vertical takeoff by direct thrust vectoring at a cost of high fuel consumption and low range and endurance.

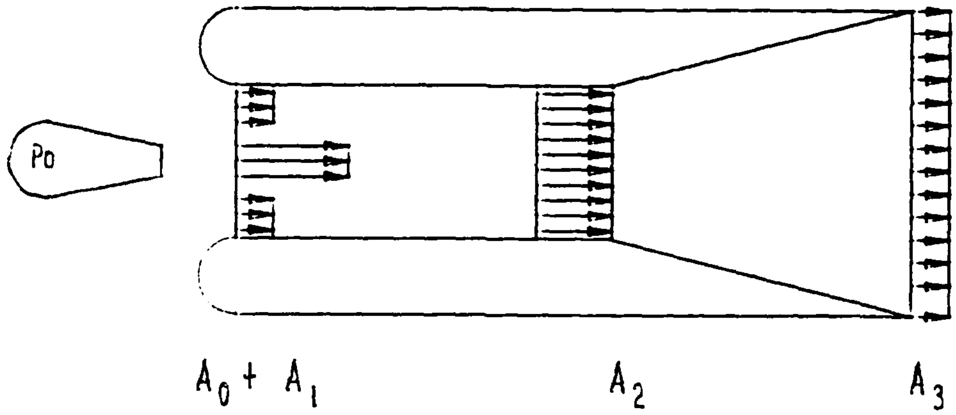

A_0 Primary Nozzle Area
A_1 Inlet Area
A_2 Mixing Chamber Area
A_3 Diffuser Exit Area

Figure 1. Center Blowing Thrust Ejector

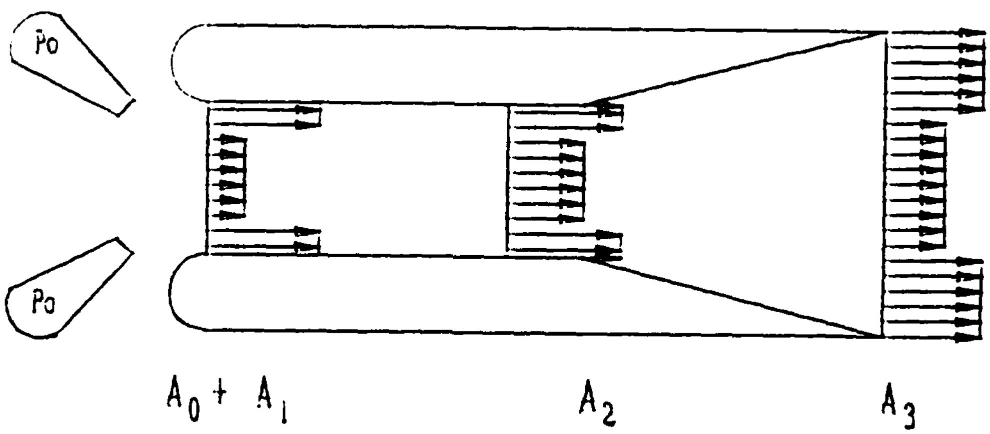

A_0 Primary Nozzle Area
A_1 Inlet Area
A_2 Mixing Chamber Area
A_3 Diffuser Exit Area

Figure 2. Wall Blowing Thrust Ejector

It is very desirable to design a V/STOL aircraft with thrust augmentation to allow sizing of the engine for proper cruise performance. So, even today, we still need to investigate all aspects of thrust augmentation.

Basic Ejector Principles

Propulsion devices develop thrust by imparting momentum to a fluid stream. A turbojet engine draws air from the atmosphere and adds energy in the form of heat by combustion. The thermal energy of a hot gas is converted to kinetic energy by accelerating it through an exhaust nozzle. A thrust augmenting ejector also adds energy useful to propulsion to air drawn from the atmosphere by the direct transfer of kinetic energy from the primary nozzle. Bevilaqua states that the mechanism of energy transfer is the turbulent mixing of the two fluid streams (3:475-481). Figure 3 shows that when a jet passes through a region where the static pressure is ΔP less than atmospheric pressure, both the primary and secondary fluids accelerate upon entering this low pressure region. The final thrust due to

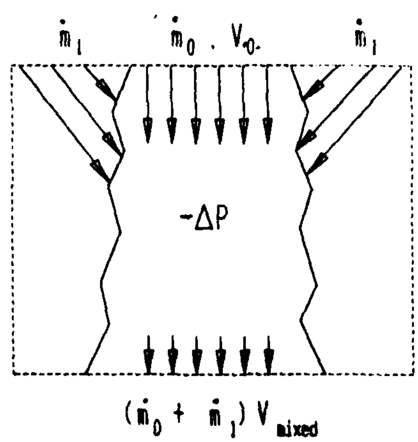

Figure 3. Jet Passing Through $-\Delta P$ Region

mixed flow is larger than the thrust due to the nozzle flow only and thrust augmentation is achieved. In an ejector, the low pressure region is produced by passing a jet through the inlet shroud. The entrained flow must accelerate and the pressure will drop even further. This low pressure region in the mixing chamber entrains the amount of secondary fluid required to assure all necessary equations of motion are met. The diffuser decreases the velocity and increases the pressure. This increase in pressure pushes against the ejector. When the mixed flow exits the ejector, it returns to ambient pressure and the overall thrust is increased.

Previous AFIT Studies

This study continues previous work done on thrust augmentation by AFIT students. Reznick studied the effects of changing the primary to inlet area ratio, diffuser exit to mixing chamber area ratio, and primary flow injection angle on thrust augmentation. He studied these effects on both a rectangular and several circular thrust ejectors (4:1-52). He showed that the thrust augmentation ratio increased as the diffuser to mixing chamber area ratio (β) increased. Reznick stated the thrust augmentation ratio peaked at $\phi = 2.07$ for $\beta = 2.6$. Unnever looked at the effect of changing the number of primary nozzles and varying the diffuser to mixing chamber area ratio (5:1-66). He showed that eight primary nozzles were superior to twelve or sixteen nozzles. He concluded the atmospheric flow entrainment was disrupted as the number of nozzles increased. Unnever achieved a thrust augmentation ratio of $\phi = 1.85$ for eight nozzles with the diffuser to mixing area ratio set at $\beta = 2.7$.

Lewis designed the current thrust augmentation test facility and data acquisition system (6:1-50). Lewis got a maximum thrust augmentation ratio of $\phi = 1.5$ using the thrust ejector configured the same as the current experiment. Lewis also showed a maximum mass augmentation ratio of $M = 10.0$ and that the mass augmentation can actually increase after the ejector has stalled and the thrust augmentation ratio is decreasing. Uhuad investigated how changes in the primary nozzle injection angle affects the thrust augmentation ratio (7:1-89). Uhuad found the optimal injection angle and height of combined for a maximum thrust augmentation ratio of $\phi = 1.6$. Uhuad found that alternating the spacing between the primary nozzle and inlet surface tends to decrease the thrust augmentation ratio. He also found diffuser blowing and suction had little effect on thrust augmentation.

Objectives

The goal of this study was to place emphasis on the relationship between mixing and thrust augmentation. An attempt was made to account for the losses in the primary nozzles, inlet, mixing chamber, and diffuser. Also attempted was a measure of the quality of the ejector. The quality of the ejector is a dimensionless measure defined later. The specific objectives of this study were:

1. Confirm the baseline established in previous studies.

2. Determine the effects of changing the inclination angle of the primary nozzle tips with respect to the inlet surface on the thrust augmentation ratio.

3. Determine the effect of primary air flow pulsing on the thrust augmentation ratio.

4. Investigate Quinn's model to account for losses and provide a measure of the effectiveness of the ejector.

Scope of Experimental Work

Testing was done with the 4.4 inch diameter circular thrust ejector previously used. The thrust ejector was tested in the thrust augmentation test facility designed by Lewis (6:1-50) and the original primary nozzles were used for baseline verification. For baseline verification, three ejector variables were changed. These variables were the nozzle injection angle (α), nozzle height (h), and nozzle exit location (θ). Figure 4 shows these ejector variables. Eight new primary nozzles with tips that could be inclined to the inlet surface were built to determine their effect on thrust augmentation. These nozzle tips were studied in four different configurations. Figure 5 highlights these four configurations. A method of injecting pulsed flow into the primary nozzles was also developed and its effect was investigated. The primary flow was pulsed at frequencies up to 15 hertz (Hz). Several computer programs were

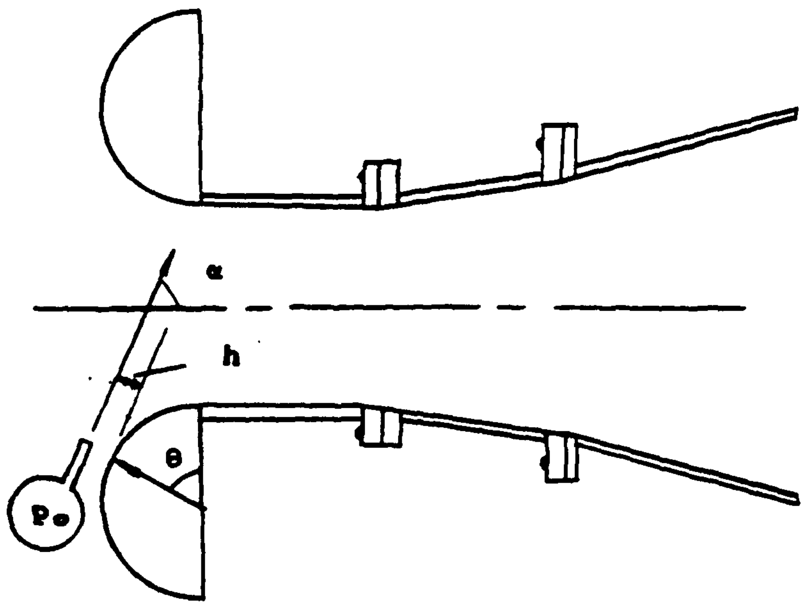

Figure 4. Thrust Ejector Variables

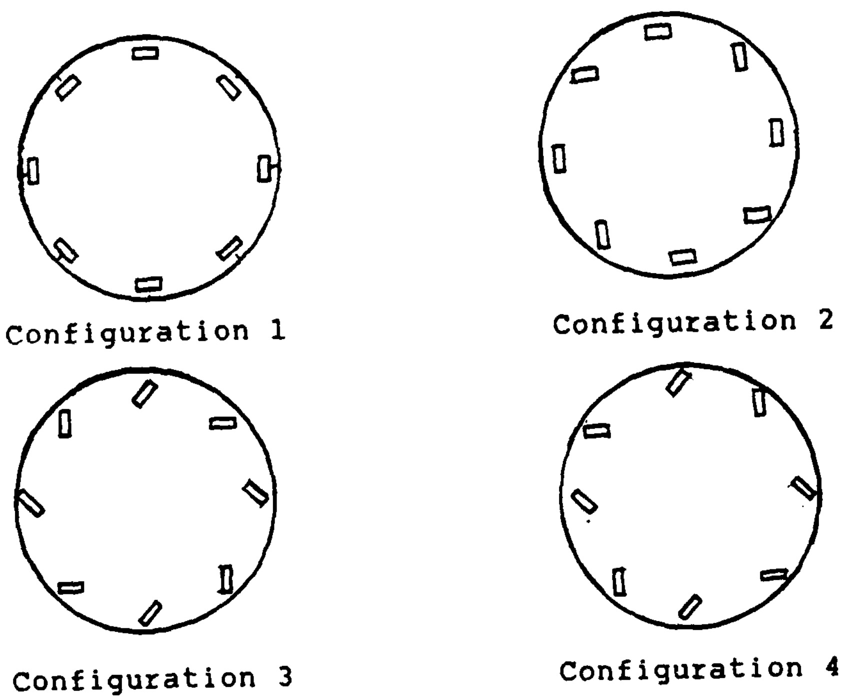

Figure 5. Four Nozzle Configurations

developed to calculate the necessary values used to account for losses and determine ejector efficiencies.

The total pressure of the primary nozzle was about 1.14 times the atmospheric pressure. The exit velocity of the primary nozzles was about 380 fps. Incompressible flow was assumed for all thrust augmentation calculations except for computing the nozzle efficiency and mass flow rate of the pulsing flow. The room ambient temperature varied between 66 and 75 ^{o}F and the variation had little effect on all calculations.

II. Theory Development

Theory Development Without Losses

In reference 1, von Karman used the basic equations of conservation of mass (continuity), momentum, and Bernoulli's equation to formulate his theory for thrust augmentation. He also assumed the flow at the exit of the mixing chamber was uniform and the fluid was incompressible. Using the conservation of mass between the entrance of the ejector and the exit of the mixing chamber for a thrust ejector without a diffuser results in the following equation:

$$V_1 (A_2 - A_0) + V_0 A_0 = V_2 A_2 \qquad (1)$$

See Fig. 6 for the control volume used in eqs. (1) and (2). The resulting equations from the conservation of momentum and Bernoulli's equation without a diffuser are as follows:

$$P_1 A_1 + P_0 A_0 + \rho V_0^2 A_0 + \rho V_1^2 A_1 = P_2 A_2 + \rho V_2^2 A_2 \qquad (2)$$

$$P_{total} = P_1 + 1/2 \rho V_1^2 \qquad (3)$$

McCormick used the above equations to develop an equation to determine V_2/V_0 only in terms of A_0/A_2. In his equation development, P_1 and V_1 were eliminated and density was assumed constant (8:280-288). This resulting equation is as follows:

$$V_2/V_0 = (-\alpha(1-2\alpha) + (2\alpha - 6\alpha^2 + 6\alpha^3 + 2\alpha^4)^{1/2})/(1 + 2\alpha + 2\alpha^2) \qquad (4)$$

where $\alpha \equiv A_0/A_2$.

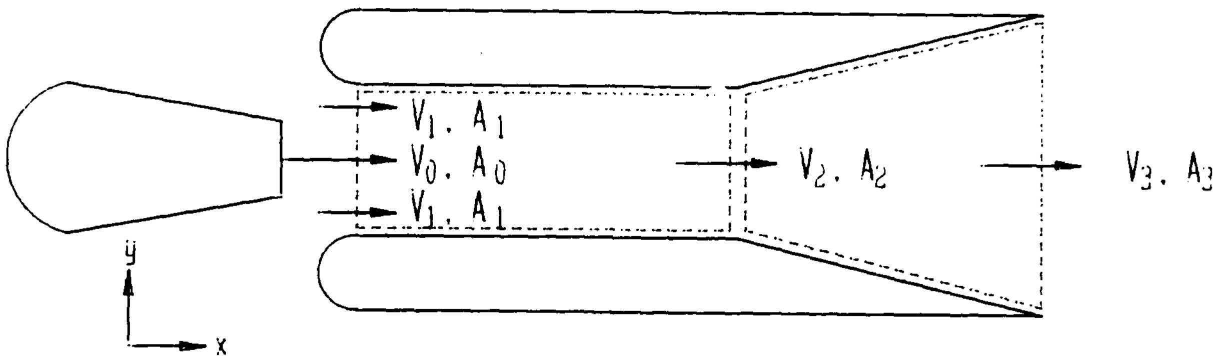

Figure 6. Control Volume of Ejector

The thrust augmentation ratio (ϕ) is defined as the ratio of the measured thrust developed to the isentropic thrust. The isentropic thrust is the thrust the nozzles would produce if the flow were expanded without losses to atmospheric pressure. The resulting equation without a diffuser is

$$\phi = \rho V_2{}^2 A_2 / \rho V_0{}^2 A_0 = (V_2/V_0)^2 (1/\alpha) \tag{5}$$

The dashed line in Fig. 7 is the result of changing α in eq. (4), determining the velocity ratio, and then finding the ϕ in eq. (5). Fig. 7 shows how the ϕ increases as $1/\alpha$ (A_2/A_0) increases if the ejector does not have a diffuser attached to the mixing chamber.

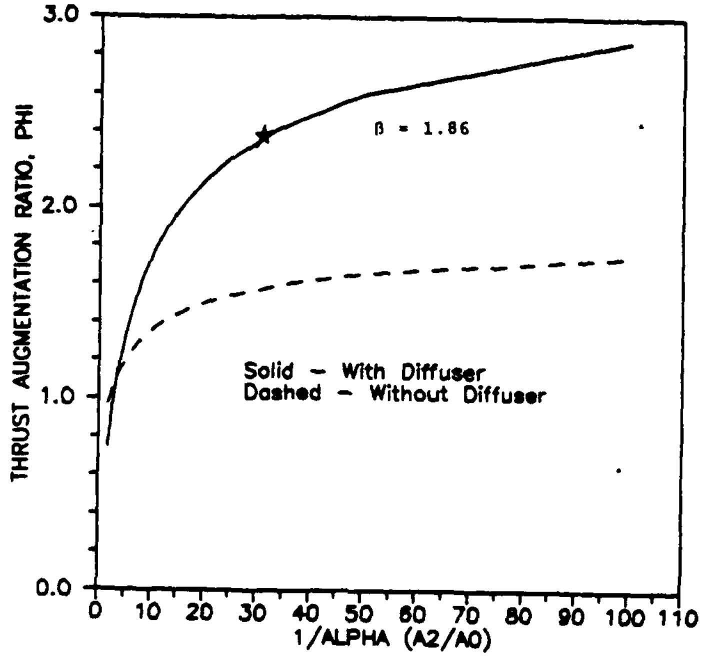

Figure 7. Thrust Augmentation Ratio vs. 1/α

The thrust augmentation ratio can be further increased with the addition of a diffuser. Again, using the equations of continuity and momentum combined with Bernoulli's equation, McCormick develops an equation for V_3/V_0. See Fig. 6 for control volume. The developed equation is as follows:

$$(V_3/V_0)^2 + (V_3/V_0)((2\alpha\beta(1-2\alpha))/(1-2\alpha+\alpha^2(1+\beta^2)) -(2\alpha-3\alpha^2)/(1-2\alpha+\alpha^2(1+\beta^2)) = 0 \quad (6)$$

The thrust augmentation ratio is now defined as

$$\phi = \rho V_3{}^2 A_3/\rho V_0{}^2 A_0 = (V_3/V_0)^2\ \beta/\alpha \quad (7)$$

where $\beta = A_3/A_2$.

The solid line in Fig. 7 shows how the thrust augmentation ratio increases when β is fixed and $1/\alpha$ is increased. Using the fixed parameters of $\alpha = 0.033$ and $\beta = 1.86$ for the thrust ejector used in the experiment, the maximum thrust augmentation ratio that can be achieved is 2.34. The star on the solid line in Fig. 7 denotes the configuration of the thrust ejector used in this experiment. Figure 8 shows how the thrust augmentation ratio varies when α is fixed and β is varied. The star on Fig. 8 also denotes the configuration of the thrust ejector used. Notice in Fig. 8 that the maximum thrust augmentation ration occurs at $\beta = 4.2$ and the ejector used for this experiment may not have been optimal.

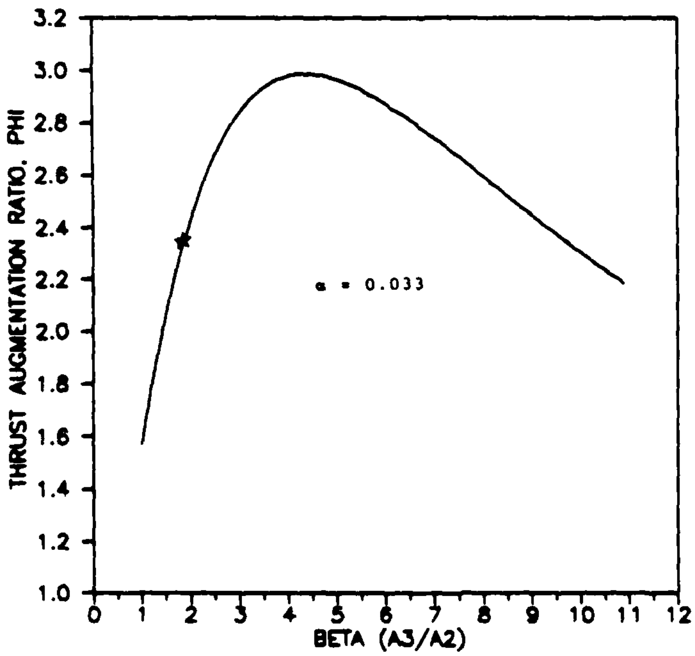

Figure 8. Thrust Augmentation Ratio vs. β

Theory Development With Losses

Quinn states that losses occur in the primary nozzles, inlet, mixing chamber, and diffuser (9:481-486). He developed a method for calculating the thrust augmentation ratio while accounting for these losses. He developed a parameter (q) to measure the quality or efficiency of the ejector. He also developed a method to determine the ideal quality value of the ejector based on its geometric properties. The quality value of the ejector increases from this ideal value as losses are incurred. Therefore, the larger the quality of the ejector, the larger the losses. He divided these losses into the following four parameters: flow skewness of the primary nozzles, primary nozzle efficiency, inlet loss coefficient, and ejector quality or performance. The equations he used to account for the losses are as follows:

$$(V_1/V_0)^2(2(A_1A_2/A_0^2) - (1+\varepsilon_1)(A_2/A_0)^2 - q(A_1/A_0)^2)$$
$$-2qV_1A_1/(V_0A_0) + 2\beta_0A_2/A_0 - q = 0 \quad (8)$$

where $\varepsilon_1 \equiv$ inlet loss coefficient
$q \equiv$ quality of ejector
$\beta_0 \equiv$ flow skewness at primary nozzle exit.

$$q = \beta_2(2\varepsilon_2+2-C_p-1/\beta_2(A_2/A_3)^2(V_e/V_3)^2) \quad (9)$$

where $\beta_2 \equiv$ flow skewness at mixing chamber exit
$\varepsilon_2 \equiv$ wall friction coefficient
$C_p \equiv$ pressure coefficient $(2(P_3-P_2)/\rho\beta_2V_2^2)$
$V_e \equiv$ velocity of moving ejector.

$$q = q_i(1+\Delta q/q_i) \quad (10)$$

where $q_i \equiv$ ideal quality of ejector $(1 + (A_2/A_3)^2)$

$$\phi = \beta_3 A_0/A_3(1+A_1V_1/(A_0V_0))^2/(1/\eta_N^2-(1+\varepsilon_1)(V_1/V_0)^2)^{1/2} \quad (11)$$

where $\beta_3 \equiv$ flow skewness at diffuser exit
$\eta_N \equiv$ primary nozzle efficiency

For this study the flow skewness at the exit of the ejector (β_3), nozzle efficiency (η_n), and thrust augmentation ratio (ϕ) were determined experimentally. These values, along with the geometric properties of the ejector, were used in equation (11) and the velocity ratio of V_1/V_0 was determined. The inlet loss coefficient (ε_1) and flow skewness of the primary nozzles (β_0) were assumed to be 0.1 and 1.0, respectively. With these values, equation (8) was used to determine a value for the quality of the ejector (q). The ideal q for the ejector used for this study is approximately $q_i = 1 + (A_2/A_3)^2$ or 1.31. With both the q and the ideal q values, $\Delta q/q_i$ was determined by using equation (10).

Bevilaqua described how to measure the skewness of the velocity profile (11:349). He defined the skewness of the flow as follows:

$$\beta_3 = \int V_3^2 dA_3/(\langle V_3\rangle^2 A_3) \quad (12)$$

where $\langle V_3\rangle \equiv \int V_3 dA_3/A_3$ is the average velocity of the flow exiting the thrust ejector.

When the flow is completely mixed, the skewness of the velocity profile is low and β_3 is equal to one. If the flow is not properly mixed, the velocity profile has curvature and β_3 has a value greater than one.

III. Facility Description

General

The experiments were accomplished using a thrust augmenter test stand and automatic data acquisition system developed by Lewis (6:1-50). This equipment provided a fast and accurate method of gathering the important data needed to analyze thrust augmentation parameters. The test stand and data collection system allow calculation of the isentropic thrust of the primary nozzles, net thrust of the ejector, mass flow rate of both the primary and secondary flows, and the exit velocity profile. The data acquisition system also provides a three dimensional velocity plot of the exit plane of the ejector. The thrust augmentation facility consists of four major components; the test stand, air supply, data acquisition system, and the ejector itself.

Test Stand

Figure 9 shows the thrust augmenter test stand with the ejector installed. The stand has a foundation of three vertical I beams bolted to the floor. The I beams are in a tripod configuration to allow installation of a frame for the pendulum mount and a flat bed for the movement of a pitot-static probe into the exit flow of the ejector. The pendulum is suspended from the vertical frame arms allowing it to swing freely. The air supply line is actually part of the frame and the pendulum. The mass flow meter is mounted

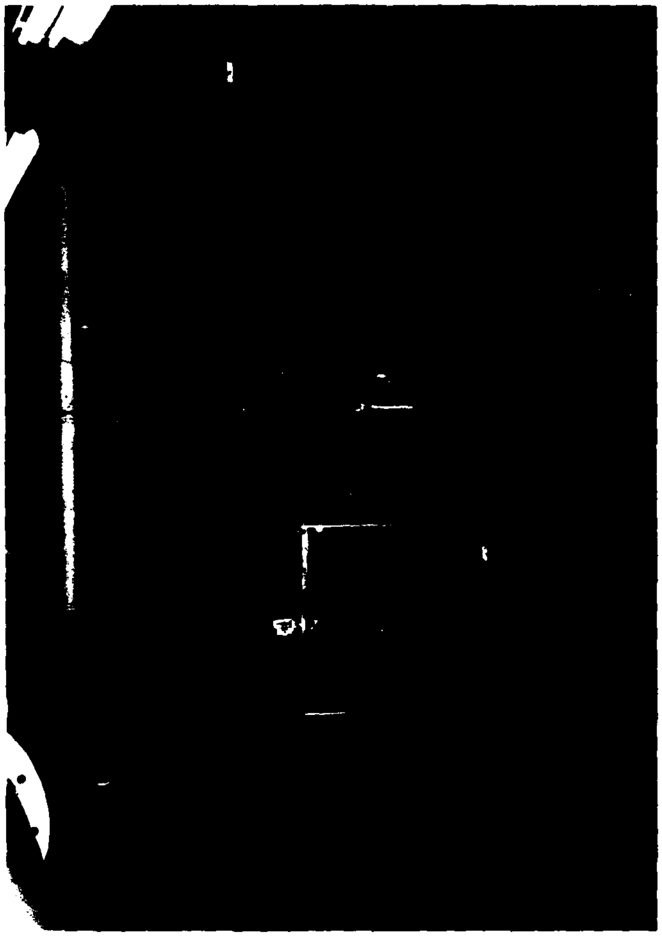

Figure 9. Photograph of Thrust Augmenter Test Stand

in the pendulum and is approximately midway between the horizontal airline and the ejector in Figure 9. The mass flow meter has a one inch orifice plate. The mass flow rate was calculated by measuring the pressure just before and after the orifice plate and using standard ASME procedures (12:156,208,233).

Figure 10 shows the pitot-static probe mounted in the traversing mechanism. The traversing mechanism allows movement in the x direction (up and down), the y direction (left and right), and the z direction (forward and backward). Movement in the z direction must be done manually just before the test is started. Movement in the x and y directions is done by computer inputs to the traversing motors. The zero values for the x and y directions are adjusted by removing the spline gears on the end of the traversing motor shafts. With the spline gears removed, the pitot-static probe can be moved to the desired position.

The net thrust of the ejector is measured by a cantilevered beam load cell. This load cell is a series of strain gages mounted to a cantilevered beam which, in turn, is mounted to a horizontal bar just below the mass flow meter. Figure 11 shows the cantilevered beam load cell. The strain gages measure the deformation of the cantilevered beam due to the thrust of the ejector and inputs that information to the data acquisition system. For each data point the thrust measurement is taken fifty times and then averaged to get a more accurate thrust value. The reason this averaging was required will be highlighted in the Results and Discussion portion of this report.

Air Supply

The primary air was obtained from the building's compressed air supply. The maximum delivery of the system is 1.0 lbm/sec at 55 psia (6:7). The system can also

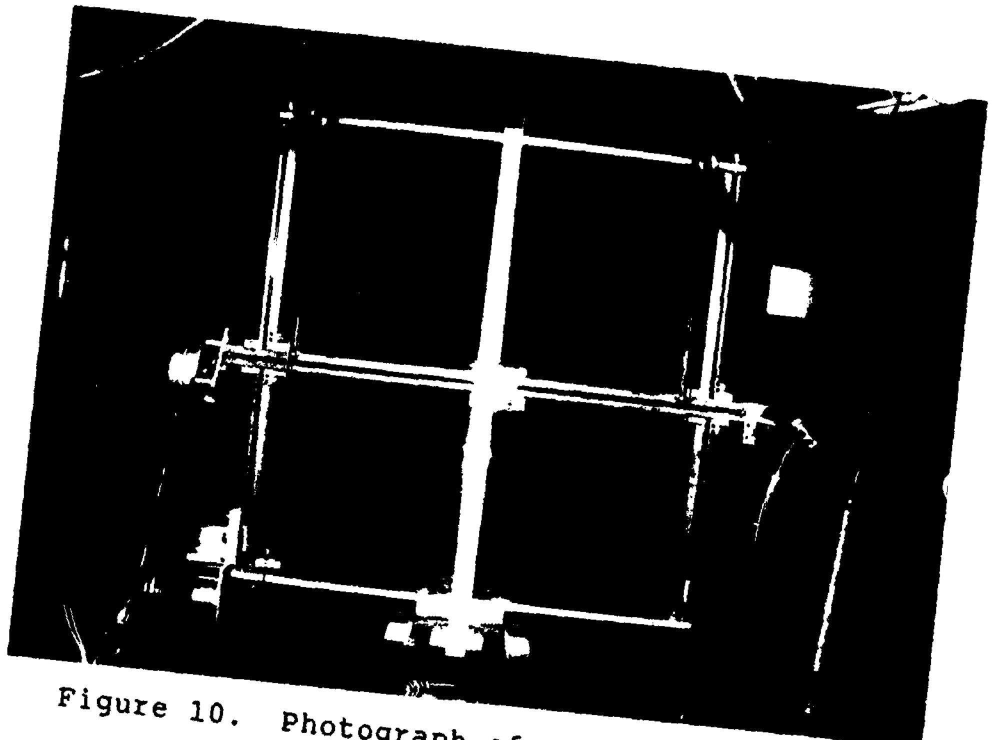

Figure 10. Photograph of Pitot-Static Probe in Traversing Mechanism

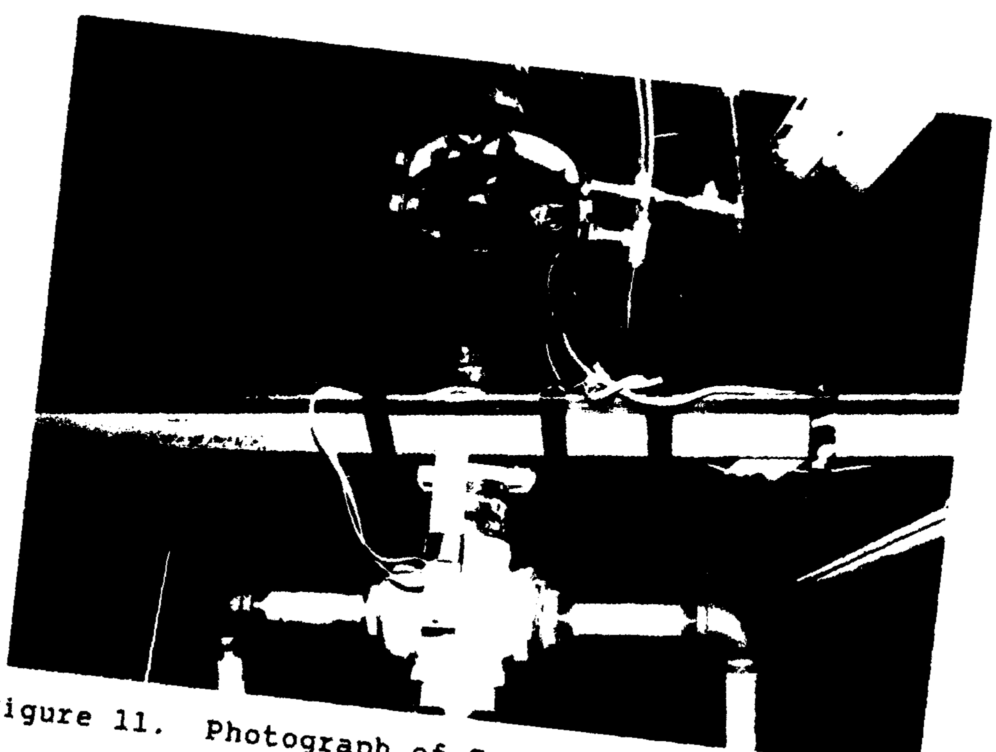

Figure 11. Photograph of Cantilevered Beam Load Cell

deliver up to 100 psia at a lower flow rate. A dome valve is installed upstream of the pendulum tee. The dome valve adjusts the pressure of the air flowing through the primary air nozzles. Figure 9 shows the dome valve upstream of the pendulum tee in the upper left hand corner of the photograph. Since the primary air nozzle pressure was only 14% greater than atmospheric pressure, the air supply easily met the test requirements.

Data Acquisition System

The data acquisition system includes a computer (HP 9845), two floppy disk drives (HP 9885M), an inkjet printer (HP 2225A), a plotter (HP 98725), a digital voltmeter (HP 722), an automatic channel scanner (HP 709), a bridge balance (CEC Type 8-108), and two digital indicators. The data acquisition system is shown in Figures 12 and 13.

Figure 12. Photograph of Data Acquisition System

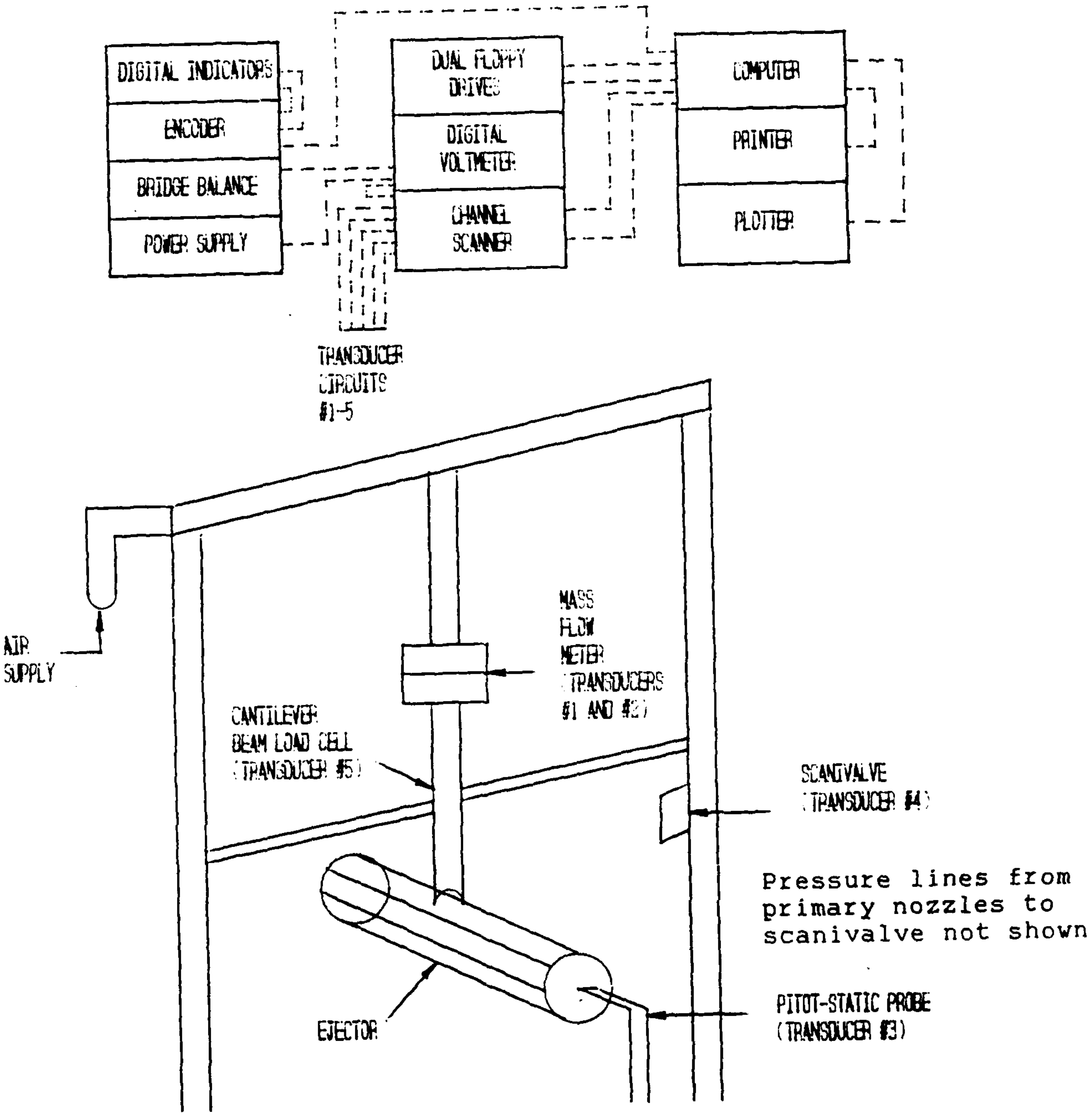

Figure 13. Schematic of Test Stand and Acquisition System

The computer monitors the inputs from four pressure transducers and the cantilevered beam load cell while controlling the positions of the scanivalve and pitot-static probe. The pressure transducers measure the pressure of the primary air before and after the mass flow orifice, the total and static pressure of the mixed air at the exit of the ejector, and the static pressure of the primary air at the exit of the nozzles. The information on these pressure transducers is as follows:

Transducers	Type	Serial #	Range	Excitation Voltage
1	CEC-1000-2	6027	0-50 psig	10.00
2	Stathem	----	0-25 psig	5.00
3	Endevco	75BF	0-5 psia	10.00
4	Scanivalve	136121	0-25 psig	5.00
5	Cantilever	-----	0-50 lbf	10.00

The scanivalve was used to monitor the static pressure of the eight primary nozzles. The computer program uses the static pressure as the total pressure (of the primary air) because of the maximum 1.14 ratio when compared to atmospheric pressure. The primary nozzles are ½ inch diameter copper tubes rounded to fit the contour of the inlet torus ring. The exit of the nozzles were pinched to a 0.065 inch by 0.96 inch opening. Each nozzle had two mounting braces soldered to them so the nozzle injection angle, height, and exit location could be adjusted. The scanivalve uses a five volt direct current power supply. The input is channeled through a SCANO solenoid controller, CTRL-S2-S6, to the scanivalve. The data acquisition program was changed from the program last used by Uhuad to make the scanivalve take a reading of the ninth pressure port. This pressure port reads atmospheric pressure and determines the drift in circuit voltage since the last calibration. This change was made to get a more accurate reading of the primary nozzle pressures.

Once the data is acquired, the computer calculates the primary mass flow using inputs from transducers 1 and 2, the thrust augmentation ratio from transducers 4 and 5, the exit velocity from the ambient temperature and transducer 3, and the mass augmentation ratio using the ejector exit velocity and the primary air mass flow. The transducers are numbered for easier referencing.

Mercury manometers were connected to all pressure lines to provide a visual display of the pressure sensed transducers connected to the data acquisition system. In the early phase of the study, manometer readings were taken and compared to the pressure readings of the transducers. This comparison showed the need for the scanivalve to sample the ambient pressure because of voltage drift of the circuit. The mercury manometers were accurate to 0.1 psi.

Ejector Description

The mounted ejector with the eight primary nozzles is shown in Figure 14. The ejector cross section is shown in Figure 15. The ejector has a 4.4 inch diameter mixing chamber with a 2 inch radius half torus mounted on the inlet

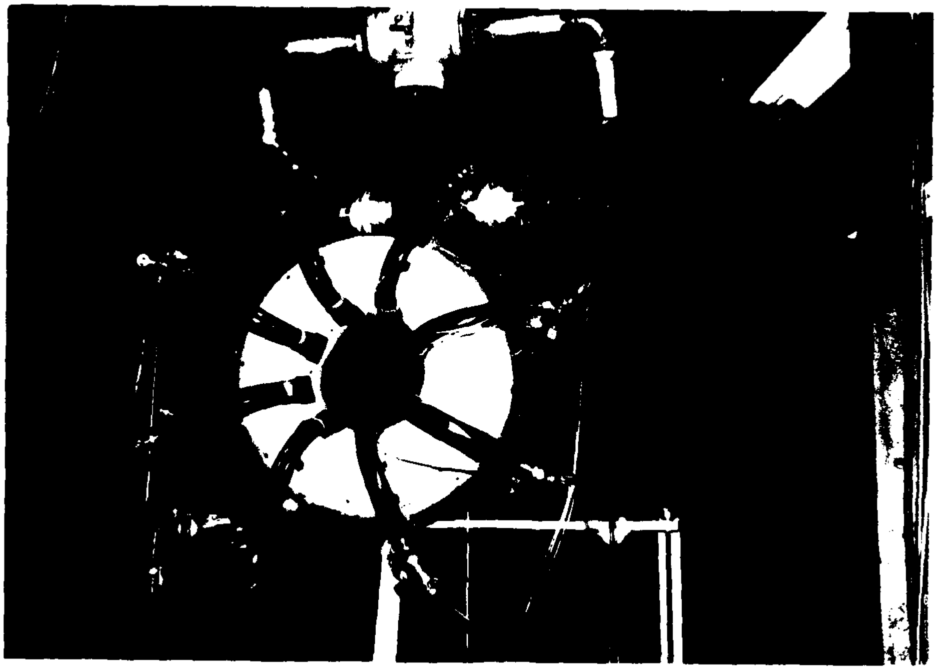

Figure 14. Photograph of Ejector With 8 Primary Nozzles

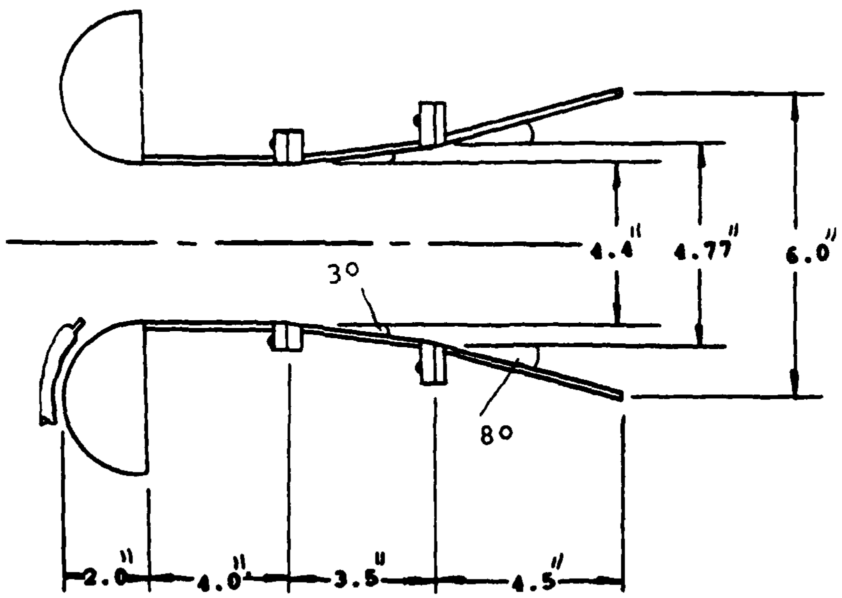

Figure 15. Thrust Ejector Cross Section

to promote smooth secondary airflow. The mixing chamber is 4 inches long. The ejector also has two discrete stages of diffusion. The first stage is 3.5 inches long and is at a 3 degree angle from the ejector centerline. The second stage is 4.5 inches long and is at an 8 degree angle from the ejector centerline. The areas and area ratios are listed in Table I.

TABLE I. Ejector Cross Sectional Areas and Area Ratios

AREAS			AREA RATIOS	
A_0	0.50	in^2	A_1/A_0 $(1/\alpha)$	30.43
A_1	14.69	in^2		
A_2	15.21	in^2	A_3/A_2 (β)	1.86
A_3	28.27	in^2		

<u>Pulsing Mechanism</u>

Primary flow pulsing was achieved by connecting four ASCO solenoid controlled valves to a power supply, function generator, and relay switch board as shown in Fig. 16. The four valves were connected to four of the primary nozzle air supply lines and pulsed at frequencies up to 15 Hz. The wave form of the pulsed flow was a square wave. Figure 17 shows how the four solenoid control valves were mounted on the thrust ejector. Figure 18 is a schematic of the flow pulsing mechanism. The air pressure upstream of the four valves was 100 psia. The diameter of the valve orifice was

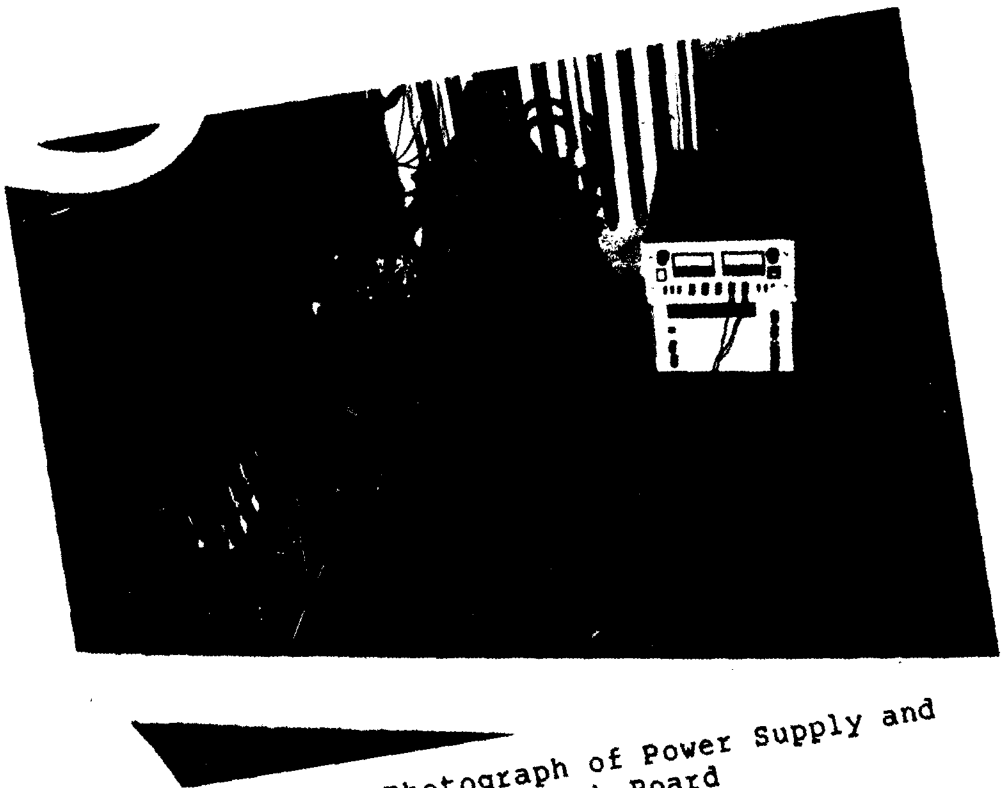

Figure 16. Photograph of Power Supply and Relay Switch Board

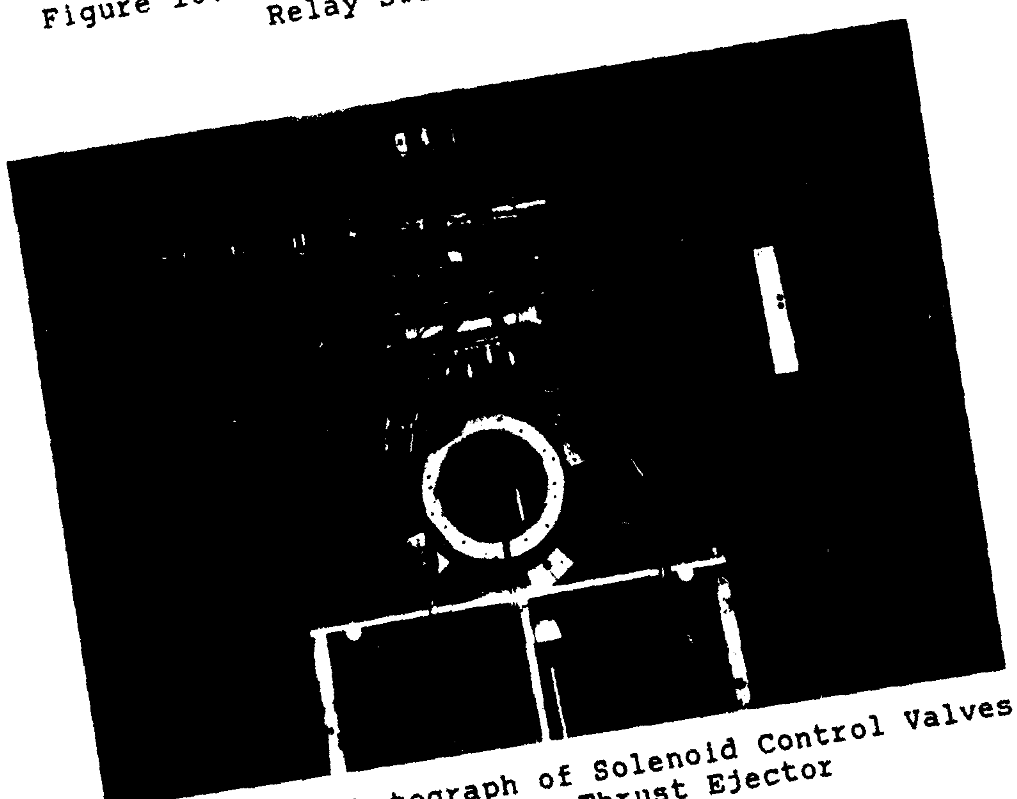

Figure 17. Photograph of Solenoid Control Valves Connected to Thrust Ejector

3/32 of an inch and choked flow was assumed. This allowed a mass flow of 0.009 lbm/sec through each valve for a total mass flow of 0.036 lbm/sec. The pulsed flow was about 30% of the total primary flow.

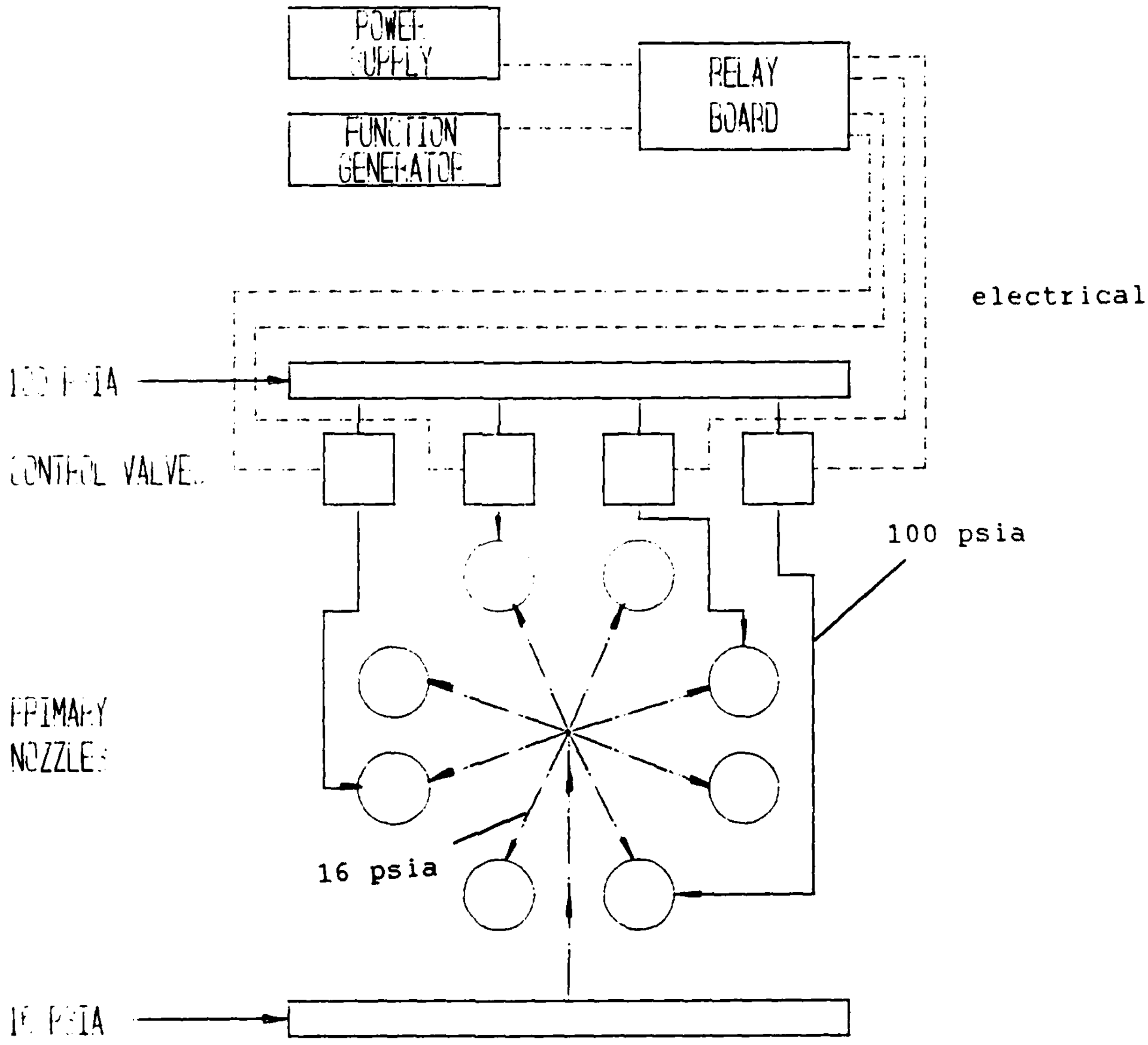

Figure 18. Schematic of Flow Pulsing Mechanism

IV. Experimental Procedures

Computer Programs

Lewis designed the test stand and developed the four computer programs for the present AFIT thrust augmentation study (6:1-50). These programs provide instructions for the computer to collect, reduce, and display the important data needed to analyze thrust augmentation of an ejector. The four computer programs are as follows:

(1) "PDUCER" - creates the calibration data for the four pressure transducers and the cantilevered beam load cell. The program places the y-axis intercept and the slopes of each transducer into a file named "PData". The data reduction program uses these values to compute the actual pressures or thrust after a data acquisition run is completed.

(2) "DATACQ" - places the scanivalve, pitot-static probe, and relay switches in their required positions to collect data. The data acquisition program asks for the necessary input information. The input information includes the x and y starting point, the x and y spacing, total number of data points, ambient temperature, and data storage file name. The data collection sequence is to sample the inputs from the transducers and move the pitot-static probe to its next position.

(3) "DREDUC" - translates the raw data collected during execution of the data acquisition program into useful information. This program calculates the primary air mass flow rate, thrust augmentation ratio, exit velocity, and mass flow ratio. The calculated information can be displayed in a specified format.

(4) "SURFAC" - plots a three dimensional picture of the velocity values at the exit plane of the ejector.

<u>Transducer Calibration</u>

The data acquisition system transducers required calibration for two reasons. The first was to keep the channel voltage from drifting away from its desired or set value. The data acquisition system uses a CEC bridge balance that, over time, allows the system voltage to drift. In some cases the reference voltage drifted from 0.0015 volts to 0.0023 volts in channel 14 (scanivalve transducer). This drift caused about a 35% error in the pressure readings. The second reason for calibration was to determine if the slope of the transducer calibration curve had changed for any reason.

The "PDUCER" computer program calibrated each of the transducers in the following sequence:

(1) Adjust excitation voltage to required value.
(2) Set reference pressure to 0.0 psi (lbf in the case of the cantilevered beam load cell).

(3) Exercise the transducer by increasing and decreasing pressure with the outside air supply regulator shown in Figure 19.

(4) Adjust the reference voltage to 0.0015 volts. This reference voltage was chosen because a lower voltage would almost always provide a 2% or larger change in the y-axis intercept value.

(5) Read and input voltage at zero reference value.

(6) Adjust pressure to maximum stated reference value.

(7) Read and input voltage at maximum reference value.

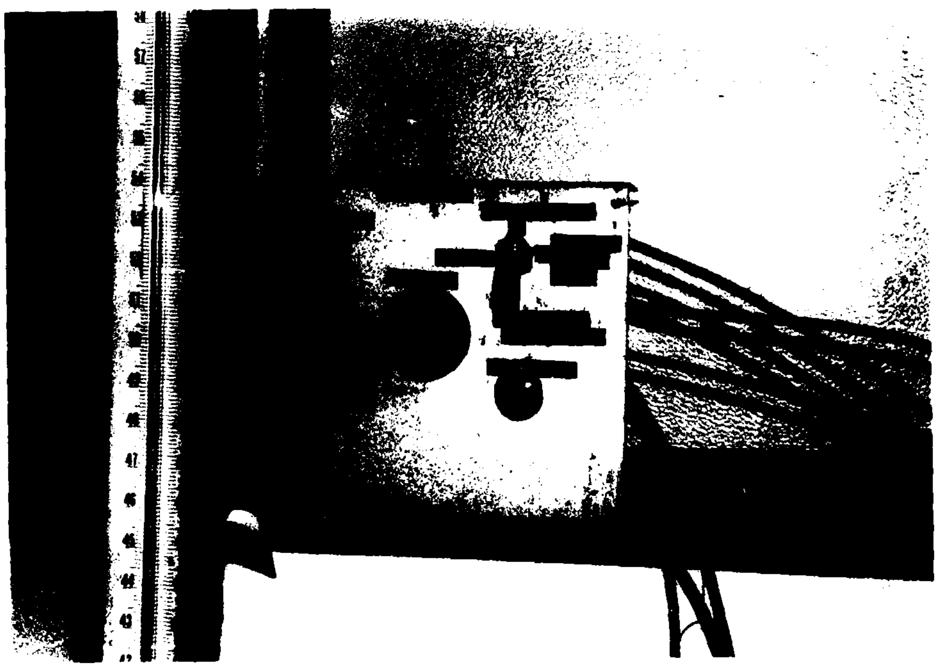

Figure 19. Photograph of Calibration Air Supply Regulator

PDUCER then calculates the y-axis intercept and slope value from the two data points. PDUCER assumes a linear relationship of pressure to voltage between the zero reference and maximum reference value. Calibration of the transducers was accomplished to assure they had linear slopes. The calibration graphs for the five transducers are in Appendix A and they were all linear except for experimental error.

Data Acquisition

The data acquisition program requests input parameters, controls the position of the pitot-static probe and the scanivalve, and collects and stores all required data. The program inputs include the number of primary nozzles, the x and y starting positions, x and y spacing, and the number of data points in the x and y direction. Additional inputs include the ambient temperature, current data storage disk number and test run number. The input data is stored in a file named "Dxxtxx" on both a primary disk and a backup disk. The primary traverse direction is determined by the number of x and y data points. If the number of x and y data points are equal, the traverser will move the pitot-static probe in the x direction first. The traverser will move to the maximum x value requested, move over the requested y space, and then move down in the x direction. This pattern will be followed until all data points have been collected. If there are more y direction data points the traverser moves in the y direction first.

Just before the traverser is moved to the starting position the program requests the operator to make sure the excitation voltage is 11.707 volts and the traverser stepper interface and SCANNER are on. When the traverser has the pitot-static probe in the proper starting position, the data acquisition can be started. The sequence of data collection is mass flow transducer #1, mass flow transducer #2, transducer #3 (pitot-static probe), transducer #4 (primary nozzle static pressure), and transducer #5 (cantilevered beam load cell). The scanivalve is stepped to sample each of the primary nozzle pressures. Figure 20 shows the scanivalve mounted to the test stand and connected to the mercury manometers. The scanivalve also samples an empty port to sample atmospheric pressure before it is homed to its reference position. The thrust measurement of the

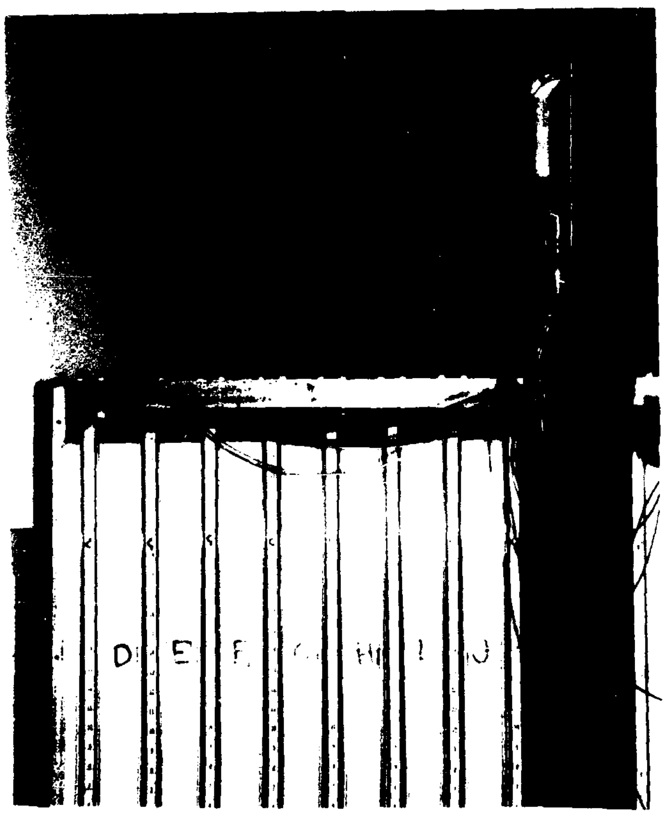

Figure 20. Photograph of Scanivalve and Manometer Board

cantilevered beam load cell is sampled fifty times per data point because of vibration of the ejector due to the fluctuation in thrust because of flow separation in the ejector. The fifty samples are then averaged to provide a thrust value. To sample the data for each channel, the voltmeter is internally triggered and entered into the appropriate data storage matrix. This data, as it is stored, is the actual voltmeter reading and will be converted to meaningful values by the data reduction program. The computer program moves the data acquisition equipment through all specified data points and then stores all raw collected data into a file named "TxxR". Again, the raw data is stored on a primary and a backup storage disk.

Data Reduction

The data reduction program reads in the data from the files labeled "DxxTxx" and "TxxR" on the primary storage disk and "PData" from the primary calibration disk. The pressure data reduction program uses the y-axis intercept (in psi units) and slope (in psi/volt units) to convert the raw collected data into engineering units. The thrust measurement is in pounds force for the y-axis intercept and pounds force/volt for the slope. The data reduction program calculates the thrust augmentation ratio (ϕ), the exit velocity , and the mass augmentation ratio. When data reduction is complete, the engineering data files are stored under "TxxE". Again, primary and backup files are made. The data reduction program allows the choice of printing the output on the screen, thermal printer, or impact printer. After printing the data the reduction program is complete.

As previously stated in chapter I, the thrust augmentation ratio (ϕ) is defined as the ratio of the measured thrust to the isentropic thrust. The measured thrust was calculated with readings from the cantilevered beam load cell. The isentropic thrust was calculated using the following equation (6:20):

$$F_i = (2\gamma)/(\gamma-1)\ A_o\ P_a((P_t/P_a)^{.286}-1) \tag{13}$$

The thrust augmentation ratio is the ratio of the measured thrust to the isentropic thrust and is as follows:

$$\phi = F_m/F_i \tag{14}$$

The ambient pressure was read while the data acquisition program was running and input into the data reduction program. The total pressure was determined by averaging the primary nozzle pressures for a given data point. The exit velocity was calculated using the ambient pressure, ambient temperature, and the pressure differential of the pitot-static probe. The following equations were used with the perfect gas equation to calculate the exit velocity:

$$V_3 = (2(P_{t3}-P_{S3})/\rho)^{1/2} \tag{15}$$

The primary air mass flow was calculated using the ambient pressure, ambient temperature, primary nozzle pressure, and the pressure readings before and after the mass flow meter. The following equations were used to calculate the primary mass flow:

$$\rho_o = (F_a + P_o)/(RT_a) \tag{16}$$

$$\dot{m}_o = 0.52\ ((c\ y\ d_2\ F_a)(\rho_1(P_1-P_2)^{½})/(1-\beta^{*4}) \tag{17}$$

Equation (17) uses standard ASME methods developed in a handbook on fluid meters (12:156,208,233). The c in equation (17) is defined as the coefficient of discharge ratio and is in units of gravity (ft/s^2). The value of c used for this experiment was 0.6062 ft/s^2 The y in equation (17) is defined as the expansion factor for air and is dimensionless. The value of y for this experiment was 0.970. The d in equation (17) is the diameter of the mass flow orifice and was one inch for this experiment. The F_a in equation (17) is the area thermal expansion factor. The value of F_a was 1.0 and was dimensionless. The β^* in equation (17) was the ratio of diameters. The value of β^* was 0.48. The pressure P_1 is the pressure of the primary flow before the orifice and the pressure P_2 is the pressure after the orifice.

The mass augmentation ratio was determined using the following equations:

$$\dot{m}_3 = \sum_{i=1}^{N} \rho_3 A_i V_i \tag{18}$$

$$\dot{m}_1 = \dot{m}_3 - \dot{m}_o \tag{19}$$

$$M = \dot{m}_1/\dot{m}_o \tag{20}$$

As shown in equation (18), the mass flow at the exit of the ejector is the summation of the incremental flow at each data point. The density of the flow exiting the ejector was assumed to be ambient density. The mass flow rate of the secondary flow is the primary mass flow rate subtracted from the thrust ejector exit mass flow rate. The mass augmentation ratio (M) is the ratio of the exit mass flow rate to the primary mass flow rate.

A sample of the printout of the final data is presented is Figure 21. The mass ratio column shows the summation of the mass augmentation ratio up to that data point. The rest of the information shows the value of the data at the time it was taken.

TEST RUN # 1 , TOTAL PRESSURE = PSIA
PAGE No. 1

Date of test(D M Y): 30 9 88 Test start time(H M): 12 8

Label data file name: D13T1
Raw data file name : T1R
Engineering units file: T1E V 8.1

Number of data points: 4
Data point array'X'spacing: .500 In Data point array'Y'spacing: 0.000 In

Number of points in X dir is: 4 Number of points in the Y dir is: 1

Pressure transducer calibration date(D M Y): 14 9 88

Room ambient temperature: 70 Room relative humidity: 70%

Ejector inlet:4.4inches Number of nozzles: 8
Components:3Deg 3.5In 8Deg 4.5In 0Deg 0.0In 0Deg 0.0In
Spacing between the nozzle and the inlet collar is: .000In

FILE NAME D13T1 VELOCITY DATA

DATA POINT	X cord. INCHES	Y cord. INCHES	Vel exit ft/sec	Thrust Ratio	Flow Primary	Flow Exit	Mass Ratio
1	.500	4.000	15.539	1.253	.058	.002	-.056
2	1.002	4.000	29.330	1.223	.058	.004	-.052
3	1.504	4.002	36.096	1.259	.057	.005	-.047
4	1.998	4.002	29.115	1.215	.058	.004	-.044

FILE NAME D13T1 PRESSURE and TEMPERATURE DATA PAGE No. 3

DATA POINTS	Ps primary PSIG	Pd orifice PSIG	Pt exit PSIG	P ambient PSIA	Thrust Lb-F	Isen THrust Lb-F
1	1.676	.449	.002	14.406	.604	.482
2	1.701	.451	.007	14.406	.584	.477
3	1.656	.440	.010	14.406	.584	.464
4	1.745	.453	.007	14.406	.592	.487

FILE NAME D13T1 PRIMARY NOZZLE DATA PAGE No. 4

POINTS	NOZ 1	NOZ 2	NOZ 3	NOZ 4	NOZ 5	NOZ 6	NOZ 7	NOZ 8
1	.499	.441	.522	.416	.504	.516	.511	.496
2	.501	.436	.520	.412	.501	.510	.501	.485
3	.488	.425	.504	.399	.485	.494	.488	.471
4	.511	.446	.530	.420	.511	.519	.511	.495

Figure 21. Sample Printout of Reduced Data

IV. Results and Discussion

General

As stated in chapter I, this study was divided into four phases. The four phases are baseline verification, a primary nozzle tip inclination study, a primary flow pulsing investigation, and an ejector performance investigation. The following details the results and discussion of these four phases.

Baseline Verification

Baseline verification was accomplished to validate the data obtained in this study and duplicate test conditions and configurations. This phase also assured the test stand, data acquisition system, and associated hardware worked properly. In this phase of the study, the injection angle (α) and height (h) between the nozzle exit and the inlet surface was varied. The third variable for this phase was the primary nozzle exit location (θ). Figure 4 shows how the three variables are defined.

Table II in Appendix B outlines the results of the baseline verification phase. Figure 22 shows the data from reference 7 along with the current study results. The dashed line is result of Uhuad's study (7:27). The solid line is the result of the current study. Both studies show the same general trend. These trends show the thrust augmentation ratio (ϕ) increases as the injection angle (α)

increases until the the maximum ϕ is reached. After maximum ϕ is reached, a further increase in α causes the ϕ to drop off rapidly.

One reason for the change in ϕ as a function of α is the flow attaches to the inlet surface and remains attached until the flow exits the ejector. If the injection angle (α) is too small, the flow hits the inlet surface and losses occur because of turbulence. If the injection angle (α) is too large, the flow will go to the center of ejector, mix with primary flow from the opposite side of the ejector, and losses occur because of turbulence and lack of flow attachment to the surface of the wall. If the injection angle (α) is optimal, the flow attaches to the surface of the wall and maximum secondary flow entrainment is achieved.

The variation of height works in much the same way as the injection angle. If the nozzle is too close to the wall surface, the expanding flow from the primary nozzle reflects off the wall and creates turbulence. If the nozzle is too far from the wall, the primary flow tends to act as a free jet and goes through the ejector without secondary flow entrainment. The change in the primary nozzle location (θ) tends to increase or decrease the length of the ejector mixing chamber as θ increases. As can be seen in Fig. 22 there is a different optimal injection angle (α) for each different θ location. Also, the maximum thrust augmentation ratio is about the same for each different nozzle location.

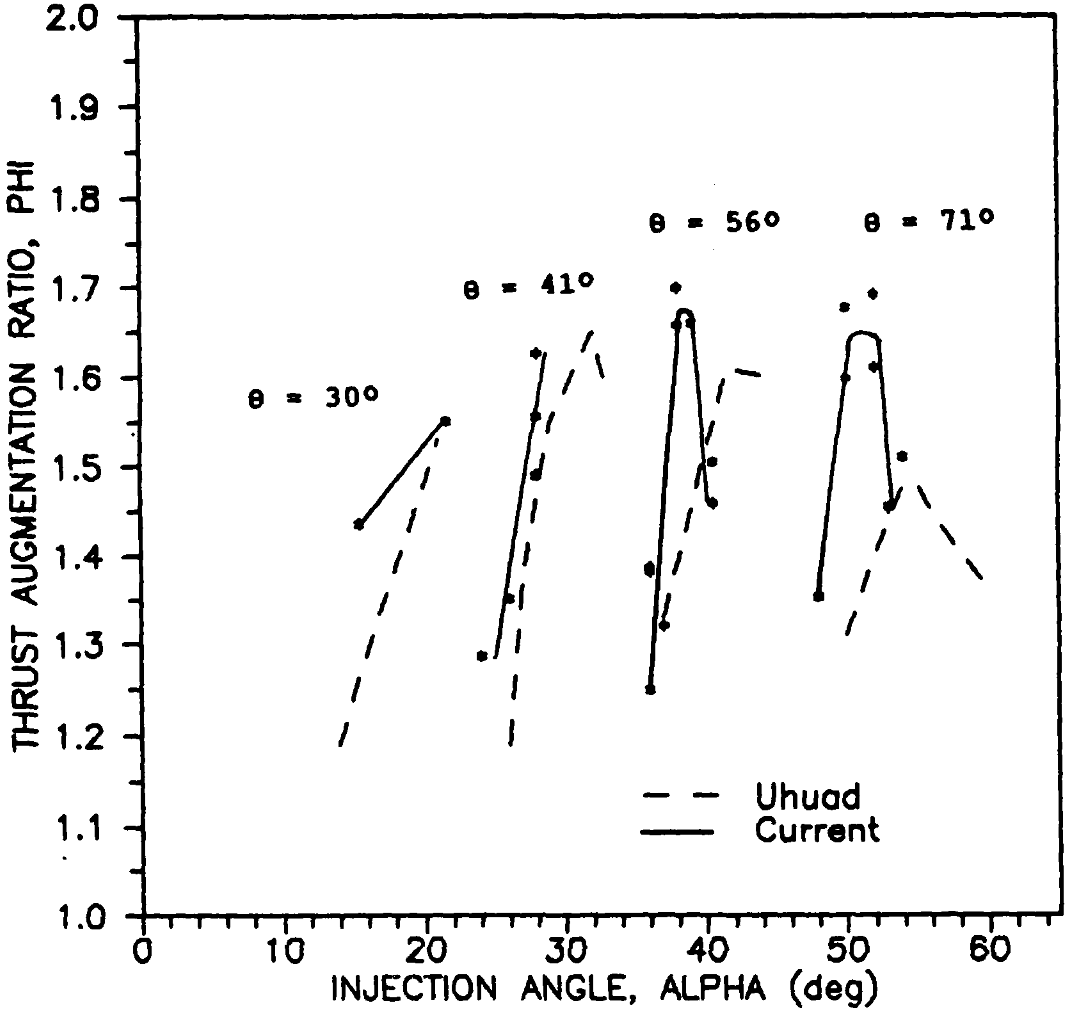

Figure 22. Thrust Augmentation Ratio Verification

This may occur because the optimal secondary flow entrainment due to viscous interaction is constant for a thrust ejector with fixed geometric properties (i.e. A_0, A_1, A_2, A_3 remain constant). Figure 23 is a plot of the optimal thrust augemntation ratio as a function of the exit nozzle location (θ). Figure 23 shows the optimal thrust augmentation ratio is about the same for every exit nozzle location.

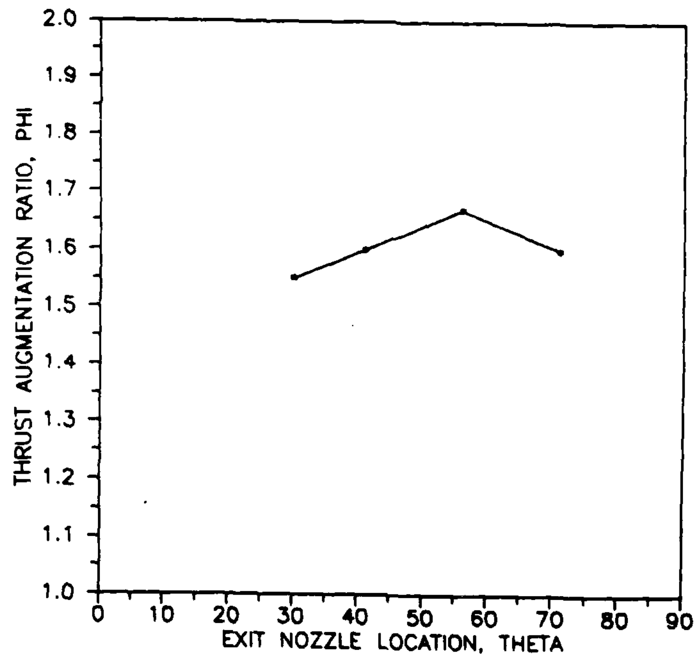

Figure 23. Optimal Thrust Augmentation Ratio as a Function of Exit Nozzle Location

Nozzle Tip Inclination

The second phase of this study investigated the effect of changing the inclination angle of the primary nozzle tips with respect to the inlet surface. Figure 5 shows the four configurations of the primary nozzle tips. The purpose of changing the primary nozzle tips in the four configurations was to study their effect on thrust augmentation and exit velocity profile. The primary nozzles were placed at three different nozzle locations. The three nozzle exit locations were $\theta = 7^{\circ}$, $\theta = 11^{\circ}$, and $\theta = 13^{\circ}$. Tables III, IV, and V in Appendix B outline the results of this nozzle tip investigation. Figures 24, 25, and 26 provide a graphical description of Tables III, IV, and V. Figures 24, 25, and 26 show that the thrust augmentation ratio is highest when the nozzle tips were set at 0° (parallel to the inlet surface of the ejector) and the flow attached to the surface wall. The solid line in Figs. 24, 25, and 26 is the thrust augmentation ratio when the nozzle tips were set at 0°. This again shows having the primary nozzles close enough to the wall to promote flow attachment is the better when compared to having the primary nozzle further from the inlet surface.

Configuration 3 was the next best configuration for the primary nozzle tip inclination. The middle sized dashed line with diamond symbols is the plot of ϕ verses α with all

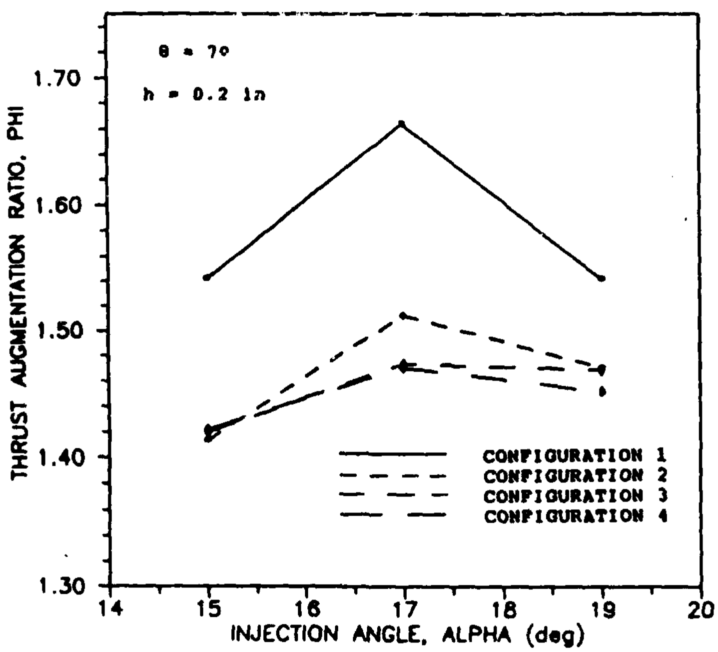

Figure 24. Effect of Nozzle Tip Inclination on Thrust Augmentation Ratio (θ = 7°)

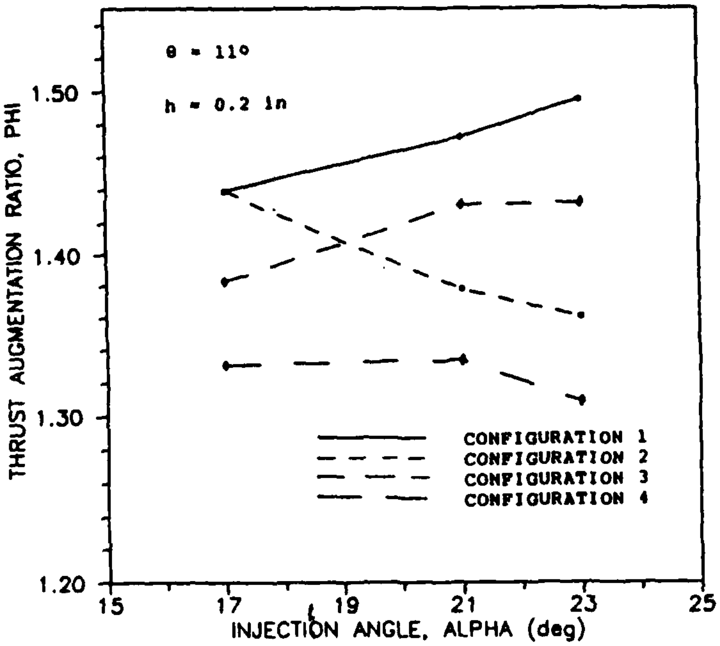

Figure 25. Effect of Nozzle Tip Inclination on Thrust Augmentation Ratio (θ = 11°)

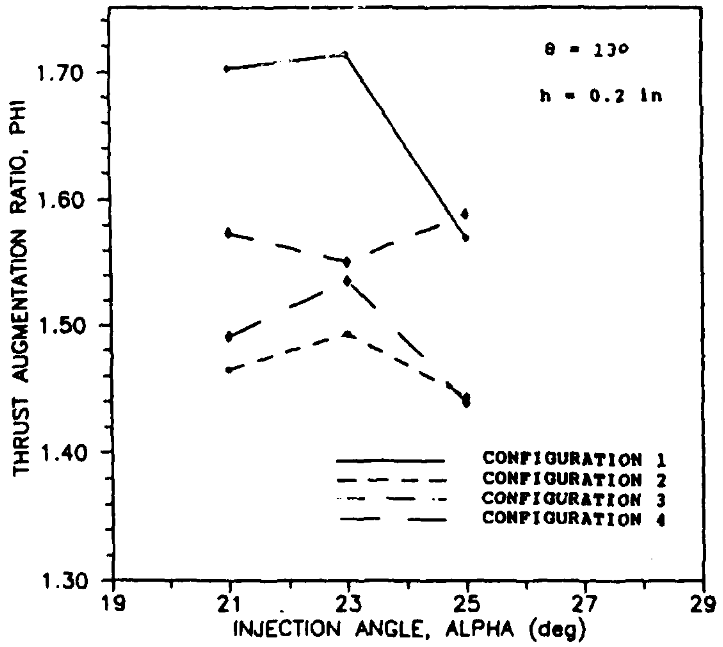

Figure 26. Effect of Nozzle Tip Inclination on Thrust Augmentation (θ = 13°)

eight nozzle tips inclined at 45° in the same direction. Figures 27, 28, 29, and 30 show exit plane velocity profiles of the four different primary nozzle configurations. Figure 27 shows the exit velocity profile with the primary nozzle set at 0°. The velocity profile shows the flow attached to the diffuser wall surface. Figure 28 shows the velocity profile with four of the primary nozzle inclined at 45° from the inlet surface. The velocity profile shows some attachment to the wall surface and a lower overall velocity average. Figure 29 shows the velocity profile with all eight of the primary nozzles inclined at 45° in the same direction. This velocity profile shows flow attachment to the bottom surface of the ejector. The average velocity in the center of the ejector is about 30 fps. The flow, however, does not attach at the top surface of the ejector and shows flow instability by the oscillating velocity values. Figure 30 shows the velocity profile of configuration 4 with half the primary flow nozzles at +45° and half at -45°. The velocity profile shows a lot of instability and lack of flow attachment at the top surface of the ejector. With this instability, the thrust augmentation ratio drops the most.

Flow Pulsing

The effect of primary flow pulsation on the thrust augmentation ratio was studied at three different heights between the primary nozzles and the ejector inlet surface. The three different heights were h = 0.20, h = 0.31, and

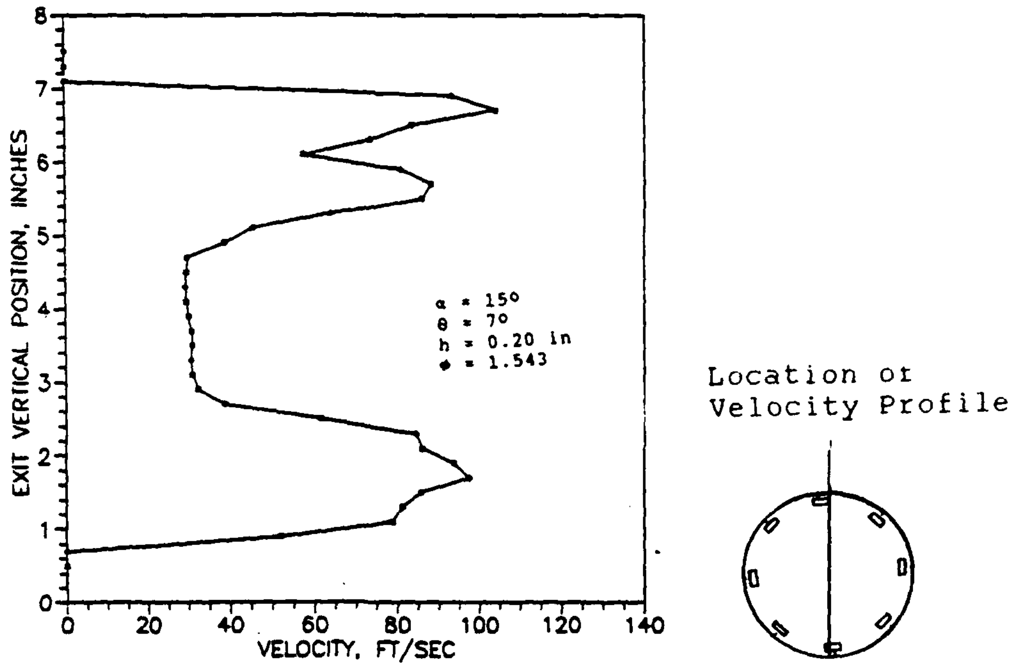

Figure 27. Exit Velocity Profile - Configuration 1

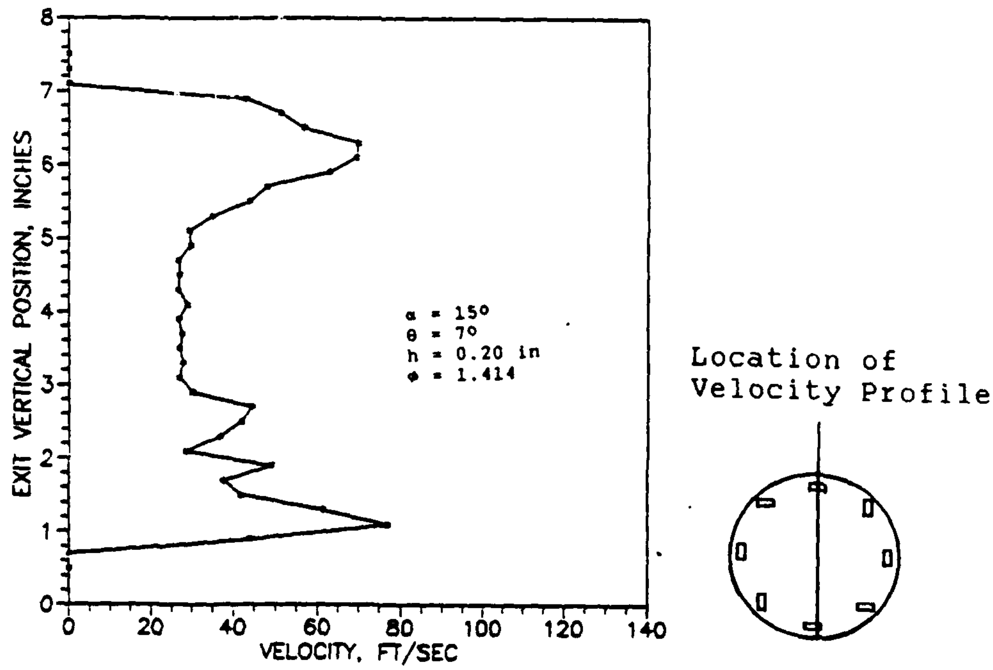

Figure 28. Exit Velocity Profile - Configuration 2

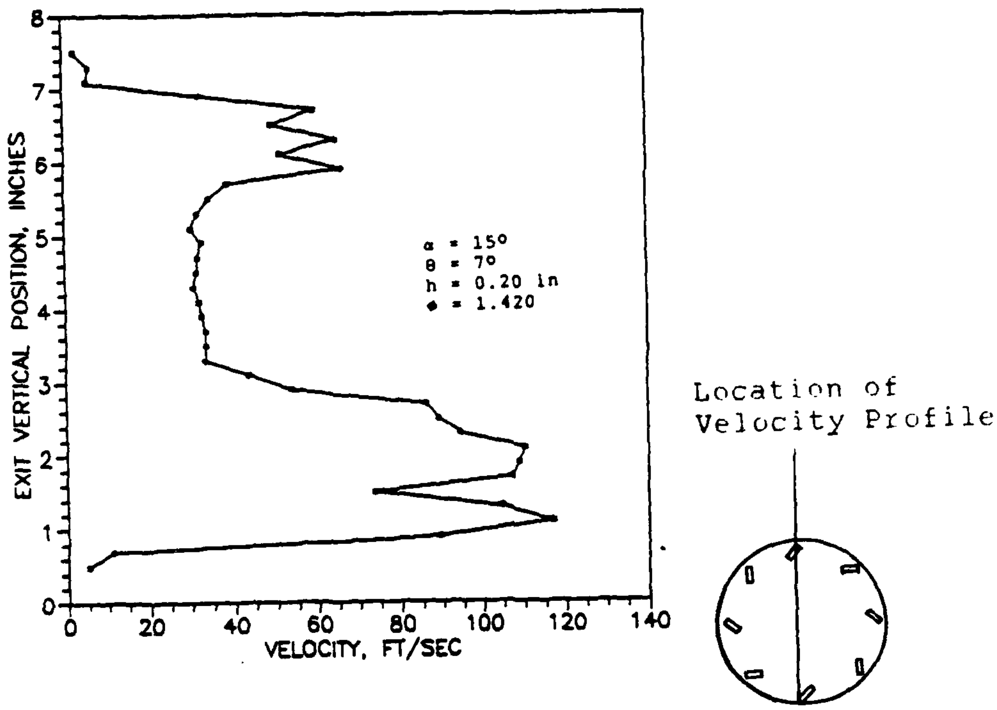

Figure 29. Exit Velocity Profile - Configuration 3

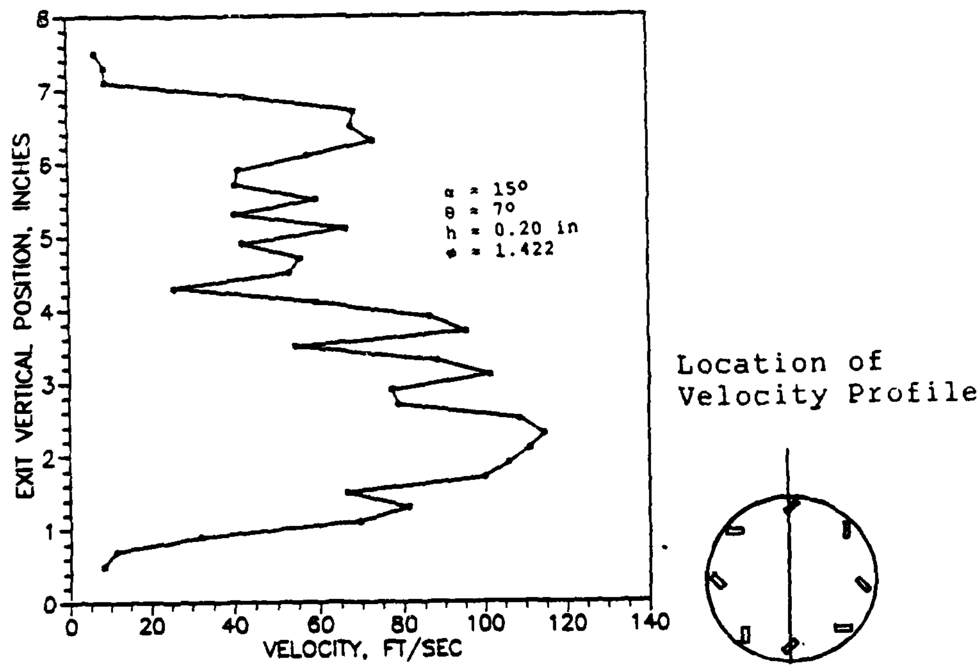

Figure 30. Exit Velocity Profile - Configuration 4

h = 0.50 inches. The flow was pulsed at frequencies of 0, 1, 2, 5, 8, 10, 13, and 15 hertz. Pulsing of the flow did add to the primary air mass flow rate. The addition of this mass flow rate was accounted for by having the same total pressure (i.e. transducer #4 had same value) in the primary nozzles when the frequency was zero. The primary air mass flow when the pulsing mechanism was running was the summation of the mass flow through the pendulum and through the control valves. Tables VI, VII, and VIII in Appendix B show the results of the primary flow pulsing study. Figures 31, 32, and 33 show the thrust augmentation ratio curve as a function of frequency. At a height of h = 0.20 inches, Fig. 31 shows that ϕ dramatically increases when the frequency changes from 0 Hz to 1 Hz. In Fig. 31 the ϕ shows an overall increase up to 15 Hz. The curve also has two dips in ϕ at frequencies of 8 and 13 Hz. A frequency of 15 Hz was not exceeded to prevent failure or overheating of the flow pulsing mechanism. Also the solenoid control valves did not properly function above 20 Hz.

Figure 32 shows the thrust augmentation ratio curve as a function of frequency at a height of h = 0.31 inches. Again, ϕ increases from 0 to 1 Hz. The trend at h = 0.31 inches is much the same as the previous curve. Like Fig. 31, Fig. 32 has two dips in ϕ at frequencies of 8 and 13 Hz. However, the maximum variation in Fig. 32 is less than in Fig. 31.

Figure 33 shows the thrust augmentation curve as a function of frequency at a height of h = 0.50 inches. The trend in Fig. 33 is the same as the two previous curves. The ϕ shows an increase with flow pulsing and a slight increase as the frequency increases. The curve in Fig. 33 also shows two dips at frequencies of 8 and 13 Hz, but the curve is much flatter than the previous curves. The maximum ϕ in Fig. 33 is 1.63 and is lower than the maximum ϕ of 1.71 at heights of h = 0.20 and h = 0.31 inches. This follows the trend that ϕ decreases as height increses.

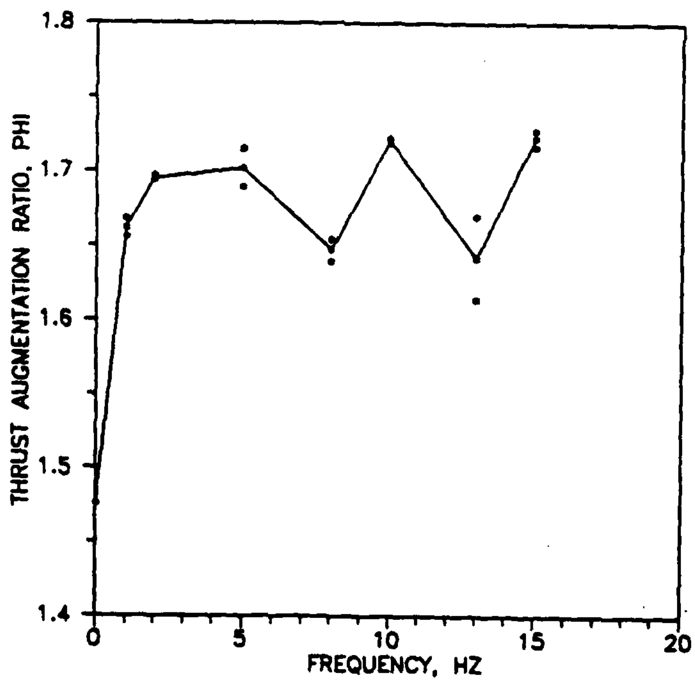

Figure 31. Thrust Augmentation Ratio vs. Frequency (h = 0.20 inches)

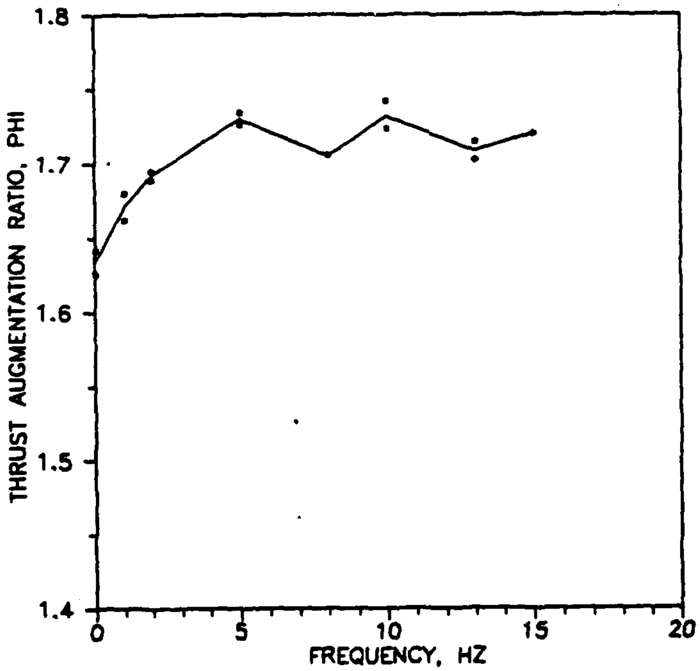

Figure 32. Thrust Augmentation Ratio vs. Frequency (h = 0.31 inches)

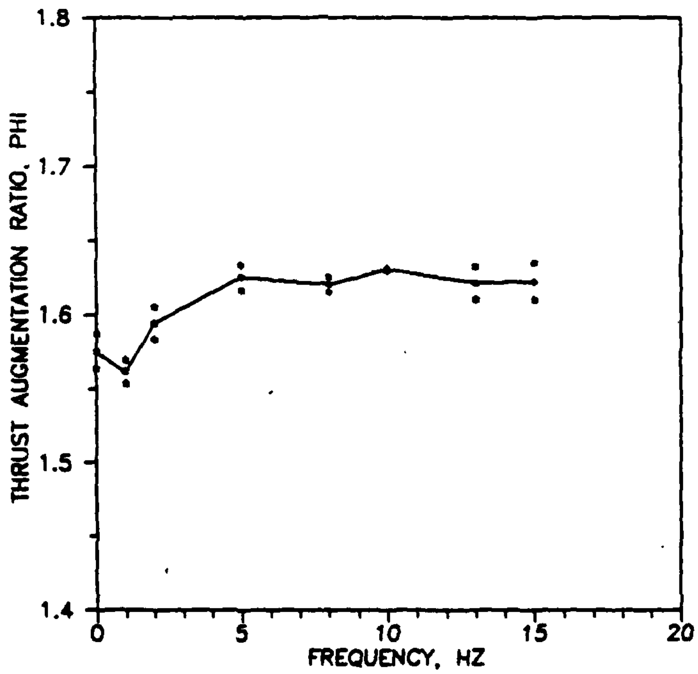

Figure 33. Thrust Augmentation Ratio vs. Frequency (h = 0.50 in)

Ejector Efficiency

Determining the ejector efficiency required the primary nozzle efficiency be determined. Table IX in Appendix B outlines the results of the nozzle efficiency test. Figure 34 shows how the nozzle efficiency varied with total pressure. The plots are centered about a value of 0.90. The original and new nozzles with movable tips were tested by placing the pitot-static probe in the exit flow. The voltage reading was taken and converted to a pressure value. This pressure value was corrected for compressible flow (12:179) with the following equation:

$$C_p = 1 + M^2/4 + M^4/24 \qquad (21)$$

The measured pressure value was converted to a velocity value. The ideal velocity value of the nozzles was calculated as if the flow expanded isentropically from the total pressure value of the primary nozzle. The nozzle efficiency is defined as the ratio of the measured kinetic energy to the isentropic kinetic energy and results in the following equation:

$$\eta_n = V_m^2/V_i^2 \qquad (22)$$

where $V_m \equiv$ measured velocity
$V_i \equiv$ ideal velocity.

Using equations (11) and (8), with a measured value of 0.90 for the nozzle efficiency and assumed values of ε_1 = 0.1 and β_o = 1.0, the value of q was calculated for the flow pulsing study. The β_3 values were determined from the exit velocity profiles. These exit velocity profiles can be found in Appendix C. The $\Delta q/q_i$ value was then determined from equation (10). Table X in Appendix B shows the results of the ejector efficiency study. Figures 35, 36, and 37 are plots of $\Delta q/q_i$ as a function of frequency at heights of h = 0.20 inches, h = 0.31 inches, and h = 0.50 inches. The solid line in Figs. 35, 36, and 37 is the difference in q from an ideal q of 1.31. The q = 1.33 value is the q value of equation (8) if no losses were assumed and the maximum thrust augmentation ratio were achieved. In Figs. 35 and 36, the solid line of $\Delta q/q_1$ vary around an average value of 0.185. The values of $\Delta q/q_1$ are much higher than those reported in Quinn's report. He reported values 0.04 for an ejector with an equivalent diffuser angle (10:10). The ejector used in Quinn's study was 50 inches long while the ejector used in this study was 14 inches long.

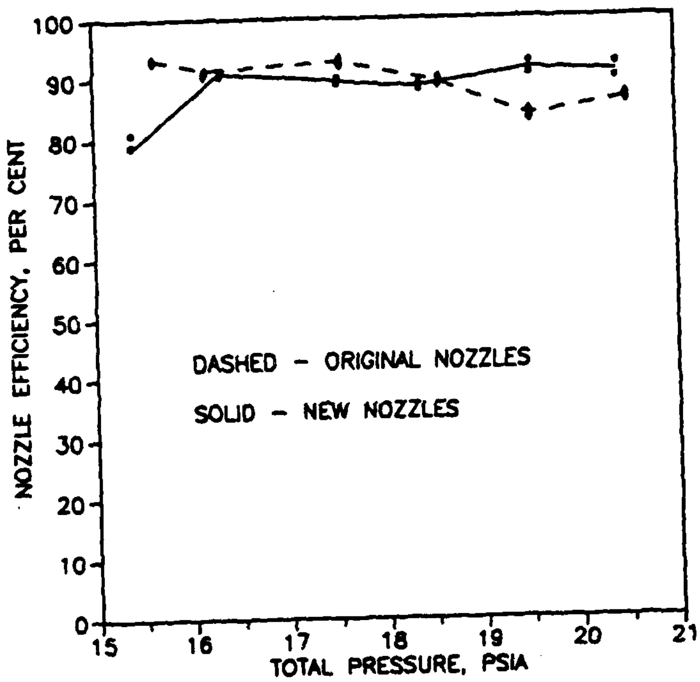

Figure 34. Nozzle Efficiency vs. Total Pressure

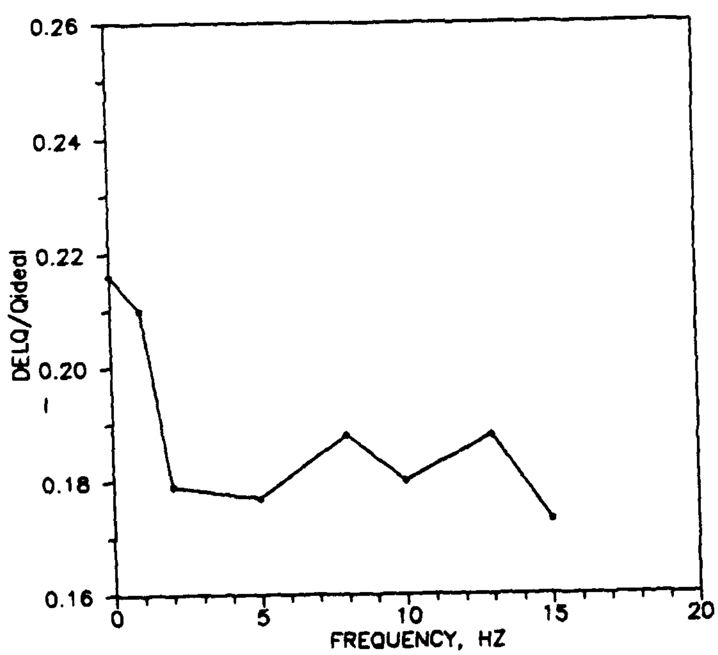

Figure 35. Thrust Ejector Losses as a Function of Frequency (h = 0.20 inches)

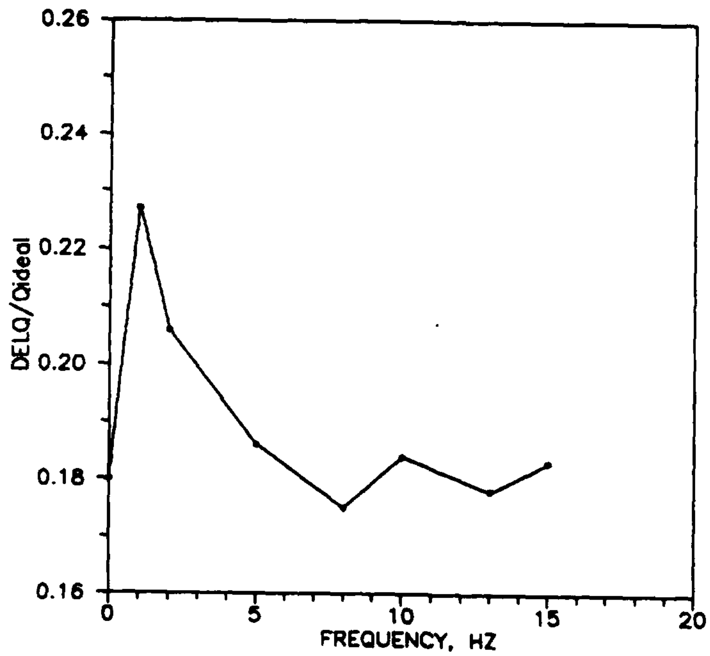

Figure 36. Thrust Ejector Losses as a Function of Frequency (h = 0.31 inches)

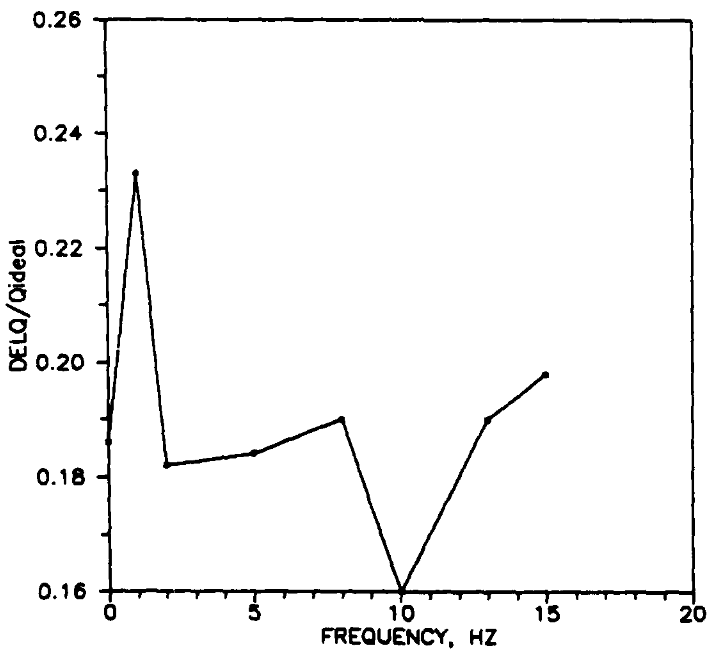

Figure 37. Thrust Ejector Losses as a Function of Frequency (h = 0.50 inches)

VI. Conclusions

The following conclusions were determined from the results of this study:

1. The thrust augmentation ratio is dependent on the primary nozzle injection angle and height. The maximum thrust augmentation value achieved was only 73% of the value that could be achieved if there were no flow losses.

2. The thrust augmentation ratio tends to decrease if the primary nozzle tips are inclined from the ejector inlet surface. Reasons for this decrease in thrust augmentation range from lack of flow attachment to the diffuser walls and losses due to friction.

3. Primary air flow pulsing did provide a higher thrust augmentation ratio and decreased ejector losses. The maximum thrust augmentation achieved with flow pulsing was 1.72 even when the injection angle was not optimal.

4. The average primary nozzle efficiency of both the original and the new nozzles was 0.90. The quality or efficiency of the 4.4 inch diameter ejector was a value of 1.56. The optimal value for the quality of the ejector was 1.31. This value was higher than values obtained by Quinn in another ejector study. However, the ejector used for this study was about four times shorter. According to Quinn, length is an important factor in thrust augmentation because complete mixing.

VII. Recommendations

Future investigations of thrust augmenting ejectors could include studies of data acquisition improvement, how thrust ejector length effects its efficiency, and the effects of primary air flow pulsing.

The improvements in the data acquisition system could include changing the computer to an IBM-PC. The computer currently supports both the thrust ejector test stand and the cascade test facility. Changing the computer to an IBM-PC would eliminate this time sharing and allow greater flexibility in calculating different augmentation parameters. Another improvement in the data acquisition system could include installing a thermocouple in the primary air pressure line for more accurate density calculations. Voltage amplifiers could be installed in the channel circuits to get larger voltages that would remove electronic noise and give greater sensitivity.

The thrust ejector could be changed in several ways. A study of thrust ejectors with different lengths for the same ratio of diffuser exit area to mixing chamber exit area could be accomplished. Different types of primary nozzles that promote hypermixing could also be studied. Further investigations of primary air flow pulsing could also be studied.

Appendix A: Transducer Calibration Graphs

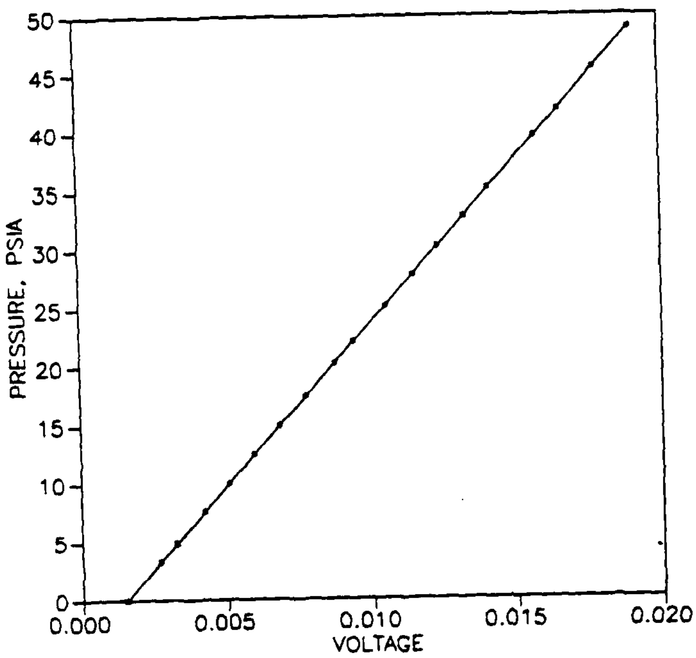

Figure A-1. Mass Flow Transducer #1 Calibration

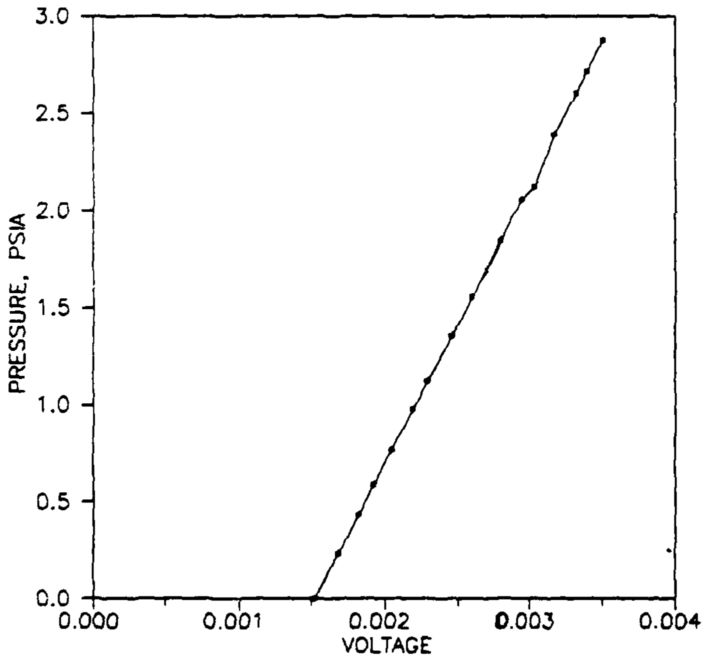

Figure A-2. Mass Flow #2 Transducer Calibration

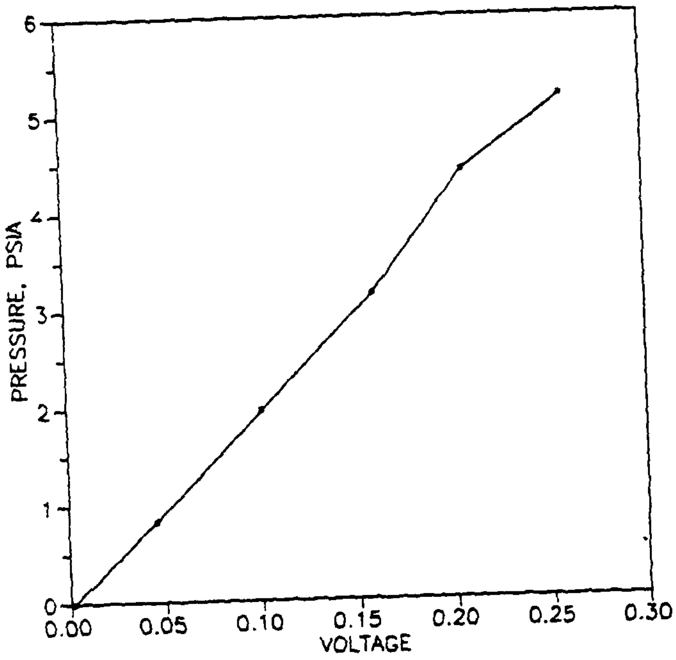

Figure A-3. Pitot-Static Probe Transducer Calibration

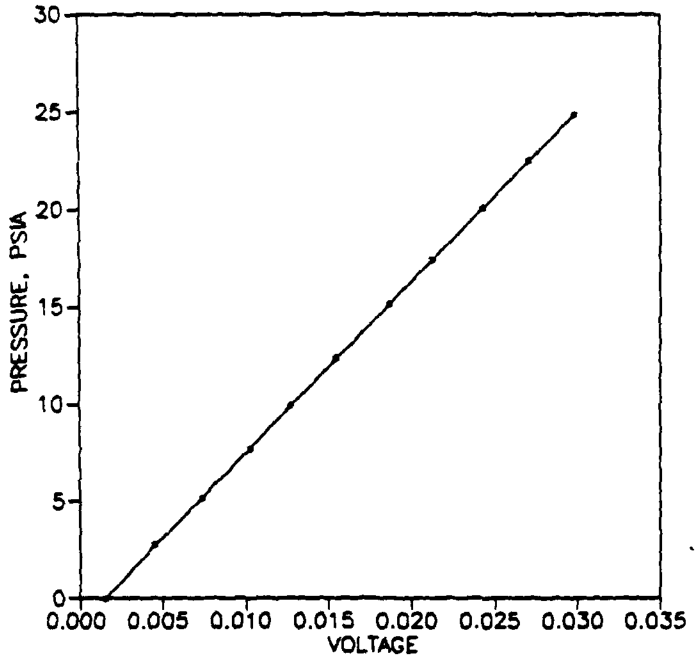

Figure A-4. Scanivalve Transducer Calibration

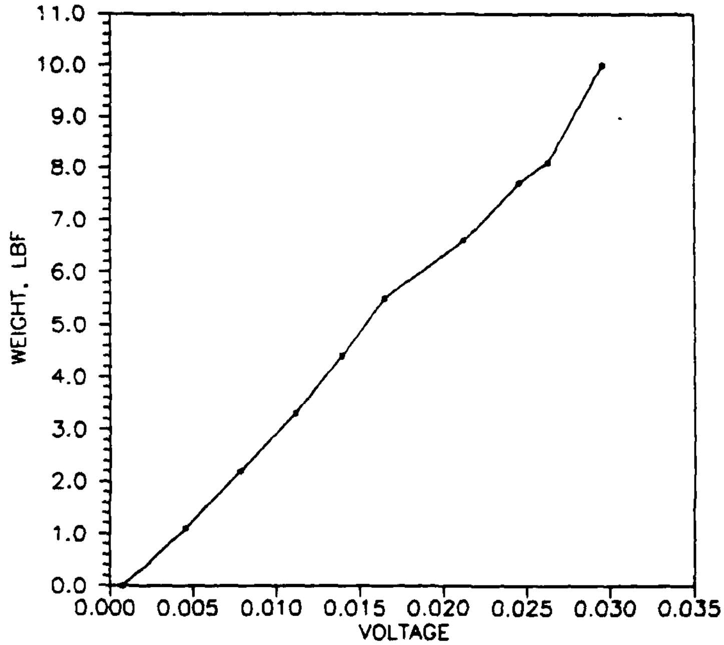

Figure A-5. Cantilevered Beam Load Cell Calibration

Appendix B: Tabulated Results

TABLE II. Baseline Verification Results

RUN #	D11T3	D11T4	D11T9	D11T10	D11T5
θ	30.0°	30.0°	42.0°	42.0°	42.0°
α	15.4°	21.6°	24.0°	26.0°	28.0°
h	0.2000	0.2000	0.1250	0.1250	0.1250
ϕ	1.436	1.550	1.286	1.350	1.626
RUN #	D11T6	D11T11	D11T15	D11T33	D11T34
θ	42.0°	42.0°	56.0°	56.0°	56.0°
α	28.0°	28.0°	36.0°	36.0°	36.0°
h	0.2000	0.2000	0.1250	0.1250	0.1250
ϕ	1.556	1.490	1.250	1.381	1.386
RUN #	D11T14	D11T31	D11T32	D11T13	D11T35
θ	56.0°	56.0°	56.0°	56.0°	56.0°
α	37.0°	38.0°	38.0°	39.0°	40.0°
h	0.1250	0.2000	0.2000	0.2000	0.2000
ϕ	1.320	1.657	1.694	1.660	1.459
RUN #	D11T36	D11T27	D11T29	D11T20	D11T28
θ	56.0°	71.0°	71.0°	71.0°	71.0°
α	41.0°	48.0°	50.0°	50.0°	52.0°
h	0.3125	0.1250	0.1250	0.1250	0.2000
ϕ	1.505	1.352	1.677	1.598	1.692
RUN #	D11T22	D11T25	D11T30		
θ	71.0°	71.0°	71.0°		
α	54.0°	53.0°	54.0°		
h	0.3125	0.3125	0.3125		
ϕ	1.454	1.454	1.510		

TABLE III. Nozzle Tip Inclination Results ($\theta = 7^\circ$)

Configuration 1			
RUN #	D11T37	D12T1	D12T7
α	15.0°	17.0°	19.0°
h	0.2000	0.2000	0.2000
ϕ	1.543	1.665	1.543
Configuration 2			
RUN #	D12T6	D12T5	D12T31
α	15.0°	17.0°	19.0°
h	0.2000	0.2000	0.2000
ϕ	1.414	1.513	1.471
Configuration 3			
RUN #	D11T38	D12T4	D12T32
α	15.0°	17.0°	19.0°
h	0.2000	0.2000	0.200
ϕ	1.420	1.474	1.469
Configuration 4			
RUN #	D12T2	D12T3	D12T33
α	15.0°	17.0°	19.0°
h	0.2000	0.2000	0.2000
ϕ	1.422	1.471	1.452

TABLE IV. Nozzle Tip Inclination Results ($\theta = 11^{\circ}$)

Configuration 1			
RUN #	D12T12	D12T8	D12T35
α	17.0°	21.0°	23.0°
h	0.2000	0.2000	0.2000
ϕ	1.440	1.470	1.490
Configuration 2			
RUN #	D12T13	D12T10	D12T36
α	17.0°	21.0°	23.0°
h	0.2000	0.2000	0.2000
ϕ	1.310	1.380	1.360
Configuration 3			
RUN #	D12T14	D12T9	D12T37
α	17.0°	21.0°	23.0°
h	0.2000	0.2000	0.2000
ϕ	1.380	1.430	1.430
Configuration 4			
RUN #	D12T11	D12T34	D12T38
α	17.0°	21.0°	23.0°
h	0.2000	0.2000	0.2000
ϕ	1.300	1.330	1.310

TABLE V. Nozzle Tip Inclination Results ($\theta = 13^\circ$)

Configuration 1			
RUN #	D12T23	D12T24	D12T40
α	21.0°	23.0°	25.0°
h	0.2000	0.2000	0.2000
ϕ	1.530	1.700	1.570
Configuration 2			
RUN #	D12T26	D12T25	D12T41
α	21.0°	23.0°	25.0°
h	0.2000	0.2000	0.2000
ϕ	1.470	1.490	1.440
Configuration 3			
RUN #	D12T39	D12T27	D12T28
α	21.0°	23.0°	25.0°
h	0.2000	0.2000	0.2000
ϕ	1.570	1.550	1.590
Configuration 4			
RUN #	D12T29	D12T30	D12T42
α	21.0°	23.0°	25.0°
h	0.2000	0.2000	0.2000
ϕ	1.490	1.540	1.440

TABLE VI. Primary Flow Pulse Results (h = 0.20 inches)

RUN #	D13T21	D13T15	D13T9	D13T14
f (Hz)	0	1	2	5
ϕ	1.476	1.668	1.697	1.689
RUN #	D13T20	D13T18	D13T13	D13T16
f (Hz)	0	1	2	5
ϕ	1.476	1.656	1.694	1.715
RUN #	D13T8	D13T19	D13T11	D13T21
f (Hz)	8	10	13	15
ϕ	1.654	1.719	1.614	1.728
RUN #	D13T10	D13T20	D13T17	D13T22
f (Hz)	8	10	13	15
ϕ	1.639	1.722	1.617	1.717

TABLE VII. Primary Flow Pulse Results (h = 0.31 inches)

RUN #	D13T18	D13T23	D13T26	D13T24
f (Hz)	0	1	2	5
ϕ	1.626	1.680	1.689	1.734
RUN #	D13T19	D13T33	D13T30	D13T31
f (Hz)	0	1	2	5
ϕ	1.642	1.662	1.695	1.726
RUN #	D13T28	D13T25	D13T27	D13T35
f (Hz)	8	10	13	15
ϕ	1.705	1.742	1.702	1.720
RUN #	D13T29	D13T34	D13T32	
f (Hz)	8	10	13	
ϕ	1.705	1.723	1.714	

TABLE VIII. Primary Flow Pulse Results (h = 0.50 inches)

RUN #	D14T16	D14T5	D14T2	D14T4
f (Hz)	0	1	2	5
ϕ	1.587	1.569	1.605	1.633
RUN #	D14T17	D14T12	D14T9	D14T11
f (Hz)	0	1	2	5
ϕ	1.563	1.550	1.583	1.616
RUN #	D14T7	D14T1	D14T3	D14T6
f (Hz)	8	10	13	15
ϕ	1.625	1.631	1.632	1.635
RUN #	D14T14	D14T8	D14T10	D14T13
f (Hz)	8	10	13	15
ϕ	1.615	1.629	1.610	1.610

TABLE IX. Primary Nozzle Efficiency Results

Original Nozzles

P_o	Volts	ΔP	Density	Vmeas	Videal	η_n
15.39	.0253	.4780	.0024527	235.34	261.49	.810
15.39	.0247	.4662	.0024527	232.42	261.49	.790
16.33	.0511	.9923	.0025478	331.05	346.09	.915
16.33	.0505	.9815	.0025478	329.24	346.09	.905
17.53	.0771	1.5117	.0027932	388.39	411.46	.891
17.53	.0779	1.5282	.0027932	390.56	411.46	.901
18.38	.0986	1.9413	.0029302	428.23	456.23	.881
18.38	.1002	1.9725	.0029302	431.61	456.23	.895
19.51	.1182	2.3320	.0031102	454.62	477.89	.905
19.51	.1207	2.3832	.0031102	459.62	477.89	.925
20.40	.1404	2.7762	.0032512	483.67	510.41	.898
20.40	.1441	2.8508	.0032512	490.10	510.41	.922

New Nozzles With Movable Tips

P_o	Volts	ΔP	Density	Vmeas	Videal	η_n
15.63	.3015	.6012	.002475	260.79	269.85	.934
15.63	.0314	.5999	.002475	260.51	269.85	.932
16.17	.0468	.9077	.002608	310.43	325.96	.907
16.17	.0471	.9137	.002608	311.46	325.96	.913
17.55	.0805	1.5789	.002779	391.85	407.87	.923
17.55	.0812	1.5943	.002779	393.76	407.87	.932
18.58	.1112	2.1920	.002942	444.35	471.28	.889
18.58	.1124	2.1690	.002942	446.85	471.28	.899
19.51	.1292	2.5520	.003089	465.86	511.35	.830
19.51	.1310	2.5890	.003089	469.22	511.35	.842
20.50	.1584	3.1361	.003245	500.03	539.20	.860
20.50	.1599	3.1650	.003245	502.35	539.20	.868

TABLE X. Ejector Efficiency Results

RUN #	D14T21	D13T15	D13T9	D13T16	D13T12
f (Hz)	0	1	2	5	8
β	1.476	1.353	1.295	1.300	1.285
V_1/V_0	0.260	0.261	0.270	0.271	0.267
V_3	65.65	61.97	59.10	58.38	56.71
q	1.599	1.591	1.551	1.547	1.563
$\Delta q/q_1$	0.216	0.210	0.179	0.177	0.188
RUN #	D13T20	D13T17	D13T21	D14T18	D13T23
f (Hz)	10	13	15	0	1
β	1.316	1.300	1.630	1.242	1.407
V_1/V_0	0.270	0.267	0.272	0.270	0.257
V_3	62.33	63.52	58.63	70.37	62.37
q	1.552	1.562	1.542	1.552	1.614
$\Delta q/q_1$	0.180	0.188	0.173	0.180	0.227
RUN #	D13T26	D13T24	D13T28	D13T34	D13T32
f (Hz)	2	5	8	10	13
β	1.360	1.341	1.288	1.326	1.305
V_1/V_0	0.262	0.268	0.271	0.269	0.271
V_3	62.39	67.71	67.27	63.46	63.54
q	1.586	1.560	1.545	1.557	1.550
$\Delta q/q_1$	0.206	0.186	0.174	0.184	0.179
RUN #	D13T35	D14T17	D14T5	D14T2	D14T11
f (Hz)	15	0	1	2	5
β	1.320	1.209	1.328	1.230	1.240
V_1/V_0	0.269	0.268	0.255	0.269	0.269
V_3	64.30	82.80	72.97	79.56	77.08
q	1.555	1.560	1.620	1.555	1.557
$\Delta q/q_1$	0.183	0.186	0.233	0.182	0.184
RUN #	D14T7	D14T8	D14T3	D14T6	
f (Hz)	8	10	13	15	
β	1.268	1.192	1.273	1.300	
V_1/V_0	0.266	0.276	0.266	0.264	
V_3	76.94	81.32	76.81	77.02	
q	1.565	1.525	1.565	1.580	
$\Delta q/q_1$	0.190	0.160	0.190	0.198	

Appendix C: Exit Velocity Plots

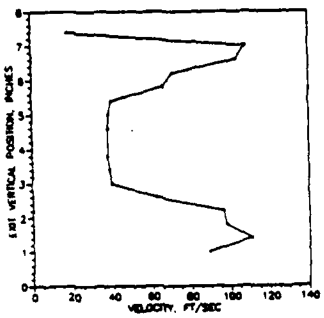

D14T21(0 Hz)

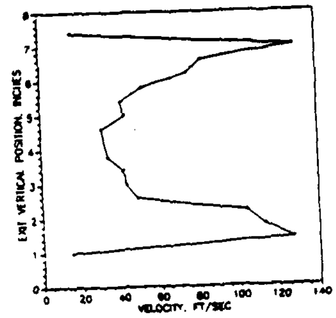

D13T15(1 Hz)

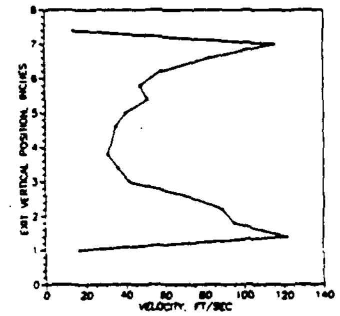

D13T9(2 Hz)

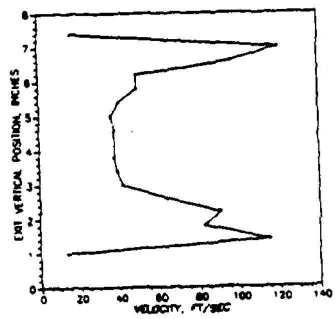

D13T16(5 Hz)

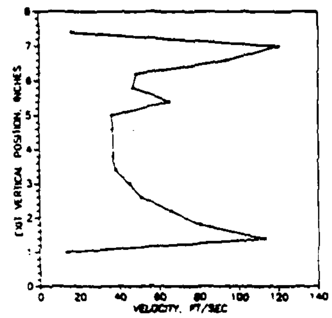

D13T12(8 Hz)

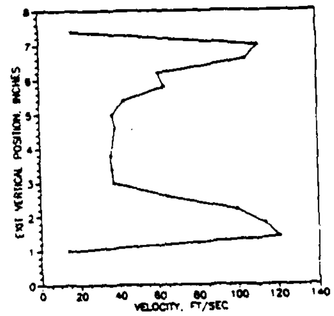

D13T20(10 Hz)

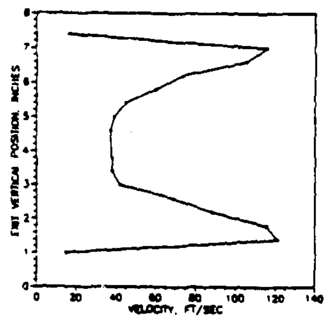

D13T17(13 Hz)

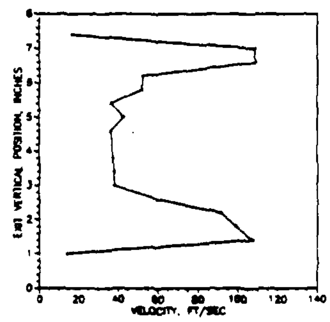

D13T21(15 Hz)

Figure C-1. Exit velocity Profiles (*h* = 0.20 inches)

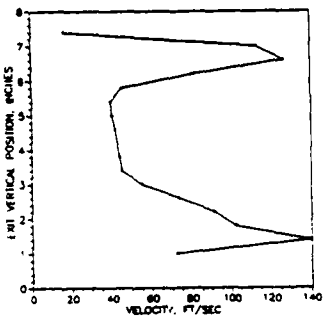

D14T18(0 Hz)

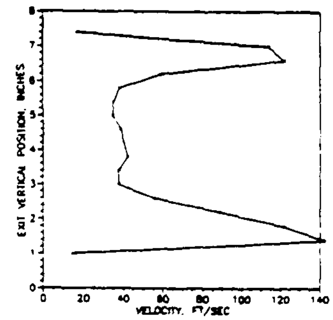

13T25(1 Hz)

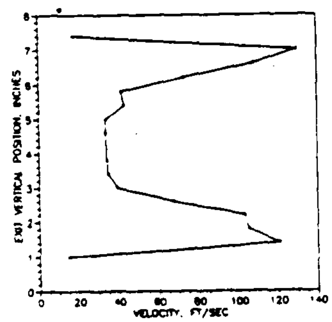

D13T26(2 Hz)

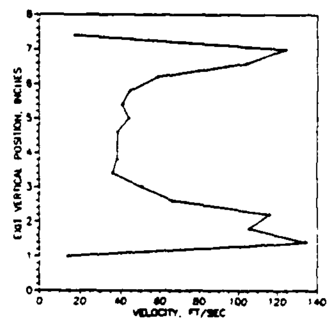

D13T24(5 Hz)

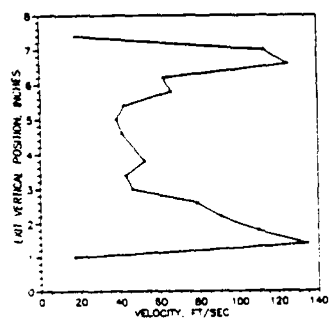

D13T28(8 Hz)

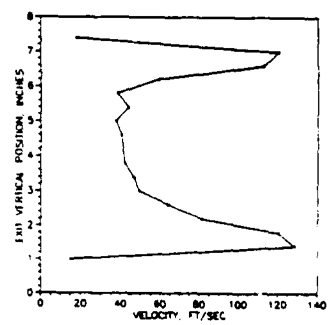

D13T34(10 Hz)

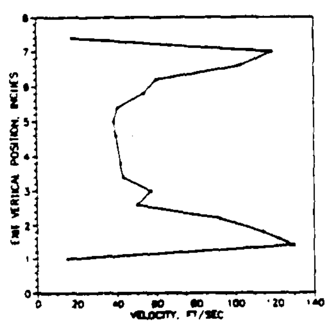

D13T32(13 Hz)

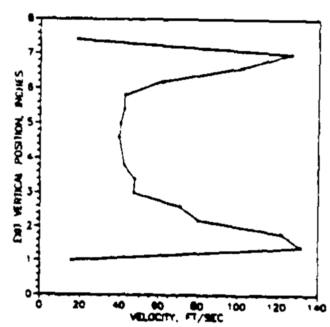

D13T35(15 Hz)

Figure C-2. Exit Velocity Profiles (h = 0.31 inches)

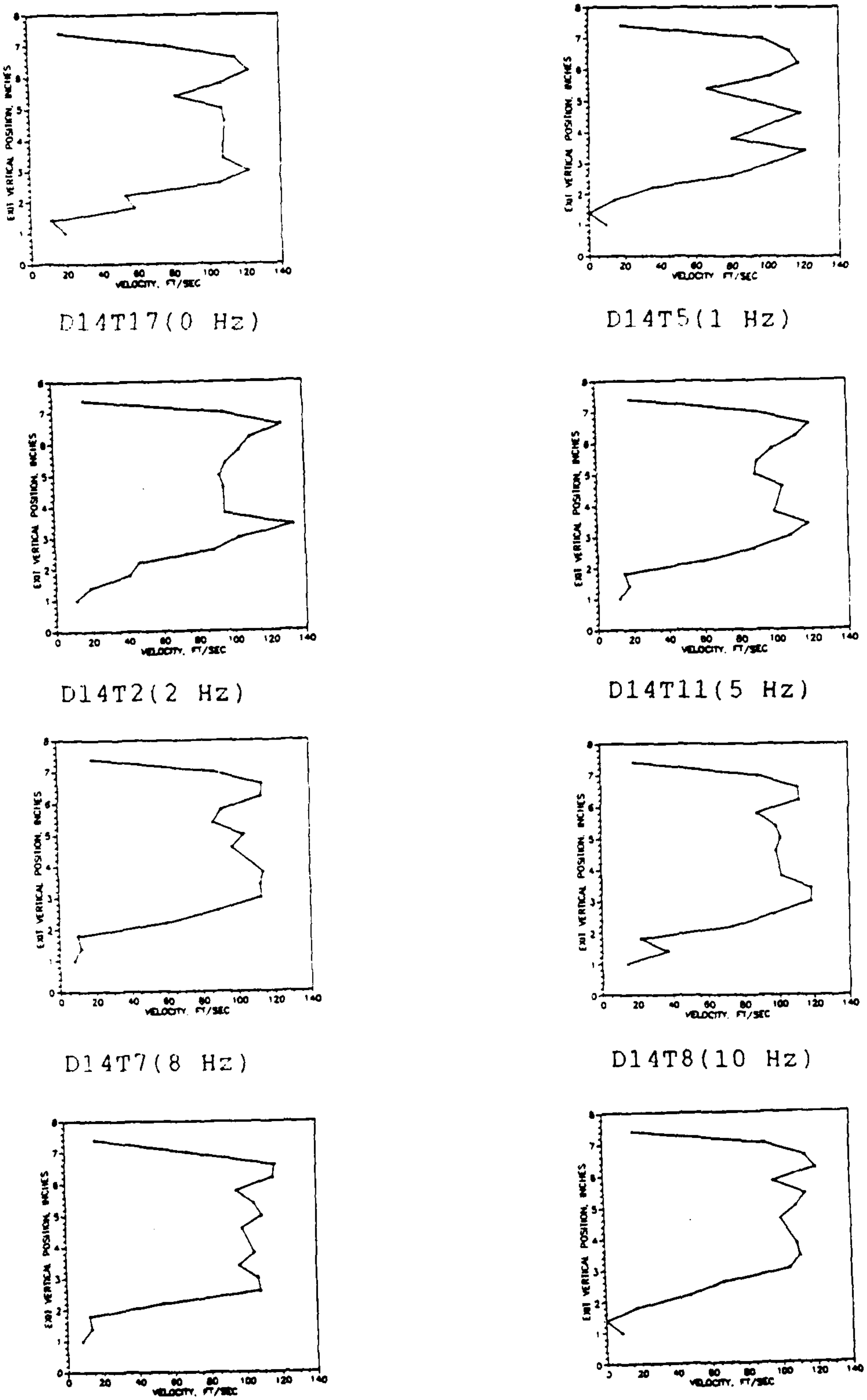

D14T17(0 Hz)

D14T5(1 Hz)

D14T2(2 Hz)

D14T11(5 Hz)

D14T7(8 Hz)

D14T8(10 Hz)

D14T3(13 Hz)

D14T6(15 Hz)

Figure C-3. Exit Velocity Profiles (h = 0.50 inches)

Bibliography

1. Von Karman, Theodore. "Theoretical Remarks on Thrust Augmentation", Contributions to Applied Mechanics, Reissner Anniverary Volume, Ann Arbor, Michigan, 1949, pp 461-468.

2. Jane's All the World's Aircraft 1985-1986, pp. 117,281.

3. Bevilaqua, Paul M. "Lifting Surface Theory for Thrust -Augmenting Ejectors", AIAA Journal 16:5, 475-481 (May 1978).

4. Reznick, Capt Steven G. An Experimental Study of Circular and Rectangular Thrust Augmenting Ejectors. MS Thesis, AFIT/GAE/AA/80D-18. School of Engineering, Air Force Institute of Technology (AU), Wright -Patterson AFB OH, December 1980.

5. Unnever, Capt Gregory An Experimental Study of Rectangular and Circular Thrust Augmenting Ejectors. MS Thesis AFIT/GAE/AA/81D-31. School of Engineering, Air Force Institute of Technology (AU), Wright -Patterson AFB OH, December 1981.

6. Lewis, Capt William D. An Experimental Study of Thrust Augmenting Ejectors. MS Thesis AFIT/GAE/AA/83D-13. School of Engineering, Air Force Institute of Technology (AU), Wright-Patterson AFB OH, December 1983.

7. Uhuad, Capt Generoso C. An Experimental Investigation of a Circular Thrust Augmenting Ejector. MS Thesis AFIT/GAE/AA/86M-3. School of Engineering, Air Force Institute of Technology (AU), Wright-Patterson AFB OH, December 1985.

8. McCormick, Barnes W., Jr. Aerodynamics of V/STOL Flight. Florida: Academic Press, Inc., 1978

9. Quinn, Brian P. "Compact Ejector Thrust Augmentation", Journal of Aircraft, 10:8 481-486 (August 1978).

10. Quinn, Brian P. Recent Developments in Large Area Ratio Thrust Augmentors. Aerospace Research Laboratories, Wright-Patterson AFB, Ohio

11. Bevilaqua, Paul M. "An Evaluation of Hypermixing for Thrust Augmenting Ejectors", Journal of Aircraft, 11:6, 348-354 (June 1974).

12. Bean, Howard S. Fluid Meters, Their Theory and Application - Volume II (Sixth Edition). New York: ASME, 1971.

13. Dwinnel James H. Principles of Aerodynamics. New York: McGraw-Hill Book Company, 1949.

VITA

Captain Donald J. Morfitt Jr. was born [redacted] He graduated from Lakefield High School, Minnesota in [redacted] and enlisted in the Air Force in August of that year. He attended technical school for jet engine maintenance at Chanute AFB, Illinois. He was assigned to the 63rd Field Maintenance Squadron working in-shop maintenance for TF-33 engines on C-141 aircraft at Norton AFB, California. In 1980, he was accepted to participate in the Airman Education Commissioning Program and attended Texas A&M University. He received a B.S. in Aerospace Engineering in December 1983 and received his commission upon graduation from Officer Training School. He was then assigned to the Ballistic Missile Office at Norton AFB, California to work on the Peacekeeper Missile. In June 1987, he entered the Air Force Institute of Technology Graduate School.

[redacted]

UNCLASSIFIED

SECURITY CLASSIFICATION OF THIS PAGE

ADA202707

REPORT DOCUMENTATION PAGE

Form Approved
OMB No. 0704-0188

1a. REPORT SECURITY CLASSIFICATION: UNCLASSIFIED

1b. RESTRICTIVE MARKINGS:

2a. SECURITY CLASSIFICATION AUTHORITY:

2b. DECLASSIFICATION / DOWNGRADING SCHEDULE:

3. DISTRIBUTION / AVAILABILITY OF REPORT: Approved for public release; distribution unlimited

4. PERFORMING ORGANIZATION REPORT NUMBER(S): AFIT/GAE/AA/88D-27

5. MONITORING ORGANIZATION REPORT NUMBER(S):

6a. NAME OF PERFORMING ORGANIZATION: School of Engineering

6b. OFFICE SYMBOL (If applicable): AFIT/ENY

7a. NAME OF MONITORING ORGANIZATION:

6c. ADDRESS (City, State, and ZIP Code):
Air Force Institute of Technology
Wright-Patterson AFB, OH 45433-6583

7b. ADDRESS (City, State, and ZIP Code):

8a. NAME OF FUNDING / SPONSORING ORGANIZATION:

8b. OFFICE SYMBOL (If applicable):

9. PROCUREMENT INSTRUMENT IDENTIFICATION NUMBER:

8c. ADDRESS (City, State, and ZIP Code):

10. SOURCE OF FUNDING NUMBERS

PROGRAM ELEMENT NO.	PROJECT NO.	TASK NO	WORK UNIT ACCESSION NO.

11. TITLE (Include Security Classification): AN EXPERIMENTAL INVESTIGATION OF FLOW MIXING ON THRUST EJECTOR EFFICIENCY(U)

12. PERSONAL AUTHOR(S): Donald J. Morfitt, Jr., Capt, USAF

13a. TYPE OF REPORT: MS Thesis

13b. TIME COVERED: FROM ________ TO ______

14. DATE OF REPORT (Year, Month, Day): 1988 December

15. PAGE COUNT: 88

16. SUPPLEMENTARY NOTATION:

17. COSATI CODES

FIELD	GROUP	SUB-GROUP
21	05	

18. SUBJECT TERMS (Continue on reverse if necessary and identify by block number):
Ejectors
Thrust Augmentation
Primary Flow Pulsing

19. ABSTRACT (Continue on reverse if necessary and identify by block number)

Thesis Advisor: Dr. Milton E. Franke
Department of Aeronautics and Astronautics

ABSTRACT ON BACK

10 Jan 89

20. DISTRIBUTION / AVAILABILITY OF ABSTRACT: ☐ UNCLASSIFIED/UNLIMITED ☒ SAME AS RPT. ☐ DTIC USERS

21. ABSTRACT SECURITY CLASSIFICATION: UNCLASSIFIED

22a. NAME OF RESPONSIBLE INDIVIDUAL: Dr. Milton E. Franke, Professor

22b. TELEPHONE (Include Area Code): 513-255-2362

22c. OFFICE SYMBOL: AFIT/ENY

DD Form 1473, JUN 86 — Previous editions are obsolete.

SECURITY CLASSIFICATION OF THIS PAGE
UNCLASSIFIED

Abstract

The purpose of this study was to determine the effect flow mixing has on the thrust augmentation of an ejector. The experimental studies were divided into four phases. The four phases were baseline verification, a nozzle tip inclination study, a primary flow pulsing study, and a study of the quality of the ejector.

The baseline verification study showed thrust augmentation is dependent upon the injection angle and height of the primary nozzles. The nozzle tip inclination study investigated the effects of having the tips inclined from the inlet surface of the ejector. The nozzle tips were inclined in four different configurations. The different configurations established a baseline or attempted to promote flow mixing and swirling. The best thrust augmentation was achieved when the nozzle tips were parallel to the inlet surface of the ejector. For the third phase, the primary air was pulsed at frequencies up to 15 hertz. The flow pulsing of the primary air enhanced flow mixing and increased thrust augmentation. The ejector efficiency study determined an approximate quality or efficiency value of the thrust ejector. When compared to an efficiency value achieved by Quinn, the ejector used in this study had four times the losses of his ejector. However, his ejector was four times longer.

Theses.